

APPLICATION OF REGIONAL MOMENT TENSOR (RMT) INVERSION PROCEDURES USING REGIONAL SEISMOGRAMS FROM THE PUERTO RICO SEISMIC NETWORK

by

Antonio E. Cameron González

A thesis submitted in partial fulfillment of the requirements for the degree of

MASTER OF SCIENCE
in
GEOLOGY

UNIVERSITY OF PUERTO RICO
MAYAGÜEZ CAMPUS
2006

Approved by:

V́ctor Huérfino, PhD
Member, Graduate Committee

Date

Carlos Mendoza, PhD
Member, Graduate Committee

Date

Eugenio Asencio, PhD
President, Graduate Committee

Date

Wilma Santiago, Arq.
Representative of Graduate Studies

Date

Johannes Schellekens, PhD
Chairperson of the Department

Date

ABSTRACT

We present the results of the application of regional moment tensor (RMT) inversion procedure within the eastern Caribbean area using regional seismograms recorded by the Puerto Rico Seismic Network (PRSN) during 2003-2006. Using data recorded over a three-year period, we estimated the source mechanisms for 6 earthquakes within the eastern Caribbean with moment magnitudes (M_w) ranging from 4.5 to 6.5. Comparisons of the computed source parameters with international agencies indicate that the RMT procedure provides an accurate estimate of the moment magnitude.

The analysis is based on the moment-tensor inversion methodology developed by Randall et al., (1995) as implemented by Mendoza (2005) to estimate the earthquake source mechanism and magnitude from seismic waveforms recorded at regional distances. This study evaluates variables, such as the velocity model and the signal-to-noise-ratio (SNR) of the recorded waveforms, and it evaluates two different bandpass filters with corner frequencies at 20- to 50-sec and 30- to 60- sec. Two velocity models were tested, the regional Caribbean model from Ewing et al., (1968) and the Preliminary Reference Earth Model (PREM) from Dziewonski and Anderson, (1981).

Our results show that using the combination of the PREM velocity model with a 30- to 60- sec bandpass filter with multiple stations improves the root-mean-square (RMS) error between the synthetics and observed waveforms. Single PRSN station inversions produce large RMS errors except at stations SJG and MPR. We observed that by changing the event depth and repeating the RMT inversion we were not able to constrain the depth of the event.

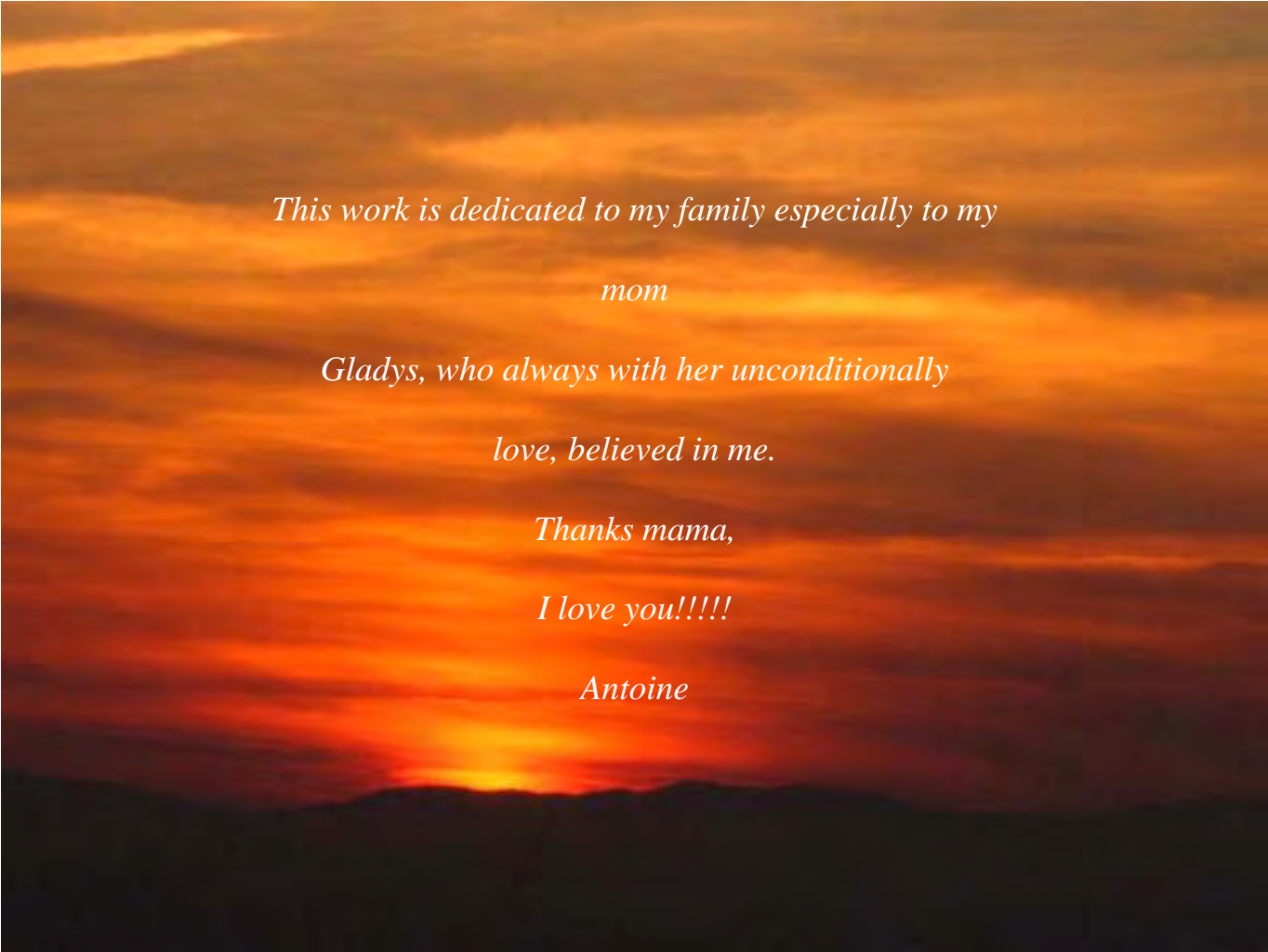
RESUMEN

Este estudio presenta los resultados de la aplicación de un procedimiento de inversión del tensor de momento sísmico regional (RMT) en la área este del Caribe utilizando sismogramas de eventos regionales registrados por la Red Sísmica de Puerto Rico (RSPR) durante los años de 2003-2006. Se estimó el mecanismo focal de 6 eventos en el área este del Caribe cuya magnitud de momento (M_w) fluctuó entre 4.5 a 6.5. Comparaciones de los parámetros determinados de la fuente con datos de agencias internacionales, indican que el tensor de momento sísmico regional provee una buena estimación de la magnitud de momento.

El análisis fue basado en la metodología de inversión del tensor de momento desarrollada por Randall et al., (1995) e implementada por Mendoza (2005) para estimar la magnitud y el mecanismo del terremoto usando formas de ondas sísmicas registradas a distancias regionales. Este estudio evalúa varias variables, como el modelo de velocidad, la razón de señal a ruido (SNR) ,y dos filtros diferentes de pasa-banda con esquinas entre 20- a 50- y de 30- a 60- segundos. Dos modelos de velocidad fueron utilizados, el modelo regional del Caribe de Ewing et al., (1968) y el “Preliminary Reference Earth Model” (PREM) de Dziewonski y Anderson, (1981).

Este estudio demuestra que utilizando la combinación de PREM con un filtro pasa-banda de 30- a 60- segundos y múltiples estaciones sísmicas, disminuye el error de “root-mean-square” (RMS) entre los sismogramas observados y los sintéticos. Inversiones con estaciones individuales de la RSPR producen errores de RMS altos con excepción de las estaciones SJG y MPR. Por último se observó que cambiando la profundidad del terremoto y repitiendo las

inversiones, el método del tensor de momento sísmico regional no fue capaz de determinar la profundidad de centroide para el terremoto.



This work is dedicated to my family especially to my

mom

Gladys, who always with her unconditionally

love, believed in me.

Thanks mama,

I love you!!!!

Antoine

ACKNOWLEDGEMENTS

This work was funded by the University of Puerto Rico Sea Grant Program (Grant # R-122-2-04). I would like to thank Mr. Sergio López for providing the logistical support at the PRSN and the IRIS Data Management Center for making available the data request through their automatic data server.

I am grateful to Dr. Víctor Huérfano, Dr. Carlos Mendoza and Christa von Hillebrandt, three of the principal investigators of the Puerto Rico-Virgin Islands Tsunami Warning System Experiment (PRVITWS), for giving me the opportunity to work in this project. I acknowledge Dr. Jay Pulliam, Dr. Hernán Santos, and Dr. John Clinton for their support and encouragement. I also acknowledge my other member of the Graduate Committee, Dr. Eugenio Asencio, for his support, encouragement and advice.

Financial support from the Puerto Rico Seismic Network and the Department of Geology at the University of Puerto Rico, Mayagüez Campus is gratefully acknowledged.

Finally, I will like to thank the PRSN staff especially to Mr. David Cuevas, Mr. Juan Lugo, Ms. Jeanette López, Ms. Yamilette Vargas, and Ms. Gisela Báez and my other fellow geology students, Alvin Bonilla, Jorge Vélez, Rafael Morales and Johanna Cepeda for their friendship and moral support during this past two years.

Table of Contents

ABSTRACT		II
RESUMEN		III
ACKNOWLEDGEMENTS		VI
TABLE OF CONTENTS		VII
TABLE LIST		VIII
FIGURE LIST		IX
1	INTRODUCTION	1
1.1	THE CIRCUM-CARIBBEAN SEISMOTECTONIC SETTING AND TSUNAMI HISTORY	1
1.2	PUERTO RICO-VIRGIN ISLANDS	6
1.3	PROBLEM STATEMENT AND OBJECTIVES	8
2	DATA AND METHODOLOGY	10
2.1	DATA	10
2.2	WAVEFORM INVERSION METHOD	13
2.3	VARIABLES TESTED AND TESTING SCHEME	14
3	RESULTS	17
3.1	TESTING SCHEME RESULTS	17
3.2	RMT RESULTS AS COMPARED TO HARVARD CENTROID MOMENT TENSOR SOLUTIONS AND THE KNOWN GEOLOGY OF THE AREA	28
4	CONCLUSIONS	37
5	RECOMMENDATIONS	38
APPENDIX A.	EVENTS AND SIGNAL-TO-NOISE RATIO ANALYSIS	44
APPENDIX B.	INSTRUMENT RESPONSES	66
APPENDIX C.	RMT INVERSION CODE	73
APPENDIX D.	CRUSTAL STRUCTURES USED IN THE REGIONAL WAVEFORMS INVERSIONS	75

Table List

Tables	Page
TABLE 2.1-1 PRSN – List of events used in this study.....	10
TABLE 2.1-2 Seismic stations used in this work.....	11
TABLE 3.1-1 RMS Errors for Event 220903 as a function of filter corner frequencies and velocity model.....	21
TABLE 3.1-2 RMS Errors for Event 060904 as a function of filter corner frequencies and velocity model.....	22
TABLE 3.1-3 RMS Errors for Event 111204 as a function of filter corner frequencies and velocity model.....	23
TABLE 3.1-4 RMS Errors for Event 181204 as a function of filter corner frequencies and velocity model.....	24
TABLE 3.1-5 RMS Errors for Event 140206 as a function of filter corner frequencies and velocity model.....	25
TABLE 3.1-6 RMS Errors for Event 020306 as a function of filter corner frequencies and velocity model.....	26

Figure List

Figure	Page
Figure 1: Map of the Circum-Caribbean region seismicity. Epicenters are for earthquakes with magnitudes >5 with focal depth shallower than 30 km (red dots), between 30- to 70- km (yellow triangles) and deeper than 70 km (inverted black triangles) from 1 January 1973 until 31 December 2005 (National Earthquake Information Center).	2
Figure 2: Seismo-Tectonic zones in the eastern Caribbean.	5
Figure 3: Tsunamis in the Caribbean region 1530-1997 (red and yellow dots). Yellow dots represent tsunamis from 1900-1997 (after Lander et al., 2002).	6
Figure 4: Bathymetric and tectonic map of the Puerto Rico, Virgin Islands, and eastern Hispaniola area showing the seismo-tectonic structures in the PRVI region. Yellow dots represent several damaging earthquakes in the PRVI region (Pacheco and Sykes, 1992). Vectors represent the relative plate motion and the plate speeds were taken from Jansma et al., (2000).	7
Figure 5: Location map of the PRSN broadband stations used in this study. Inverted red triangles represent realtime CMG-3T sensors. Black triangles are realtime CMG-3ESP sensors; blue star represents a STS-1 sensor that belongs to the Global Seismic Network (GSN).	11
Figure 6: Comparison of the deconvolved vertical ground velocities observed at each PRSN broadband station used in this study for the Mw 8.7 Sumatra event of March 2005 with the deconvolved vertical ground velocity record from the GSN station SJG. (A) Raw deconvolved vertical ground velocities (B) 50- to 100-s bandpass filtered deconvolved vertical ground velocities.	12
Figure 7: P-wave velocity profile used in this study; (A) the Caribbean velocity model after Ewing et al., (1968) and, (B) the PREM model (Dziewonski and Anderson, 1981).	14
Figure 8: Example of the Signal-to Noise Ratio analysis for the 092203 Dominican Republic event recorded at PRSN broadband station MPR. Also showing: (a) the 3-component waveforms, (b) the pre-event noise window, (c) the signal window, and (d) the corresponding amplitude spectra, where the signal amplitude spectrum is shown in red, and the pre-event noise amplitude spectrum is shown in black.	18
Figure 9: Source-depth analysis for our database. Velocity model as well the passband corner frequencies used are shown to the left of each row. Each column represents an example of hypocentral depth values for single and multi stations.	27
Figure 10: Source mechanism, magnitude and fault planes solutions obtained for the 22 Sep 2003 earthquake using the RMT technique at a fixed depth of 10 km compared with the HRV moment tensor solution. Synthetic (red line) and observed (blue line) records are shown given for each component (vertical, radial and tangential). The station code, the distance from the source to the station in kilometers and the azimuth from the source to the station are shown above the waveforms.	30
Figure 11: Source mechanism, magnitude and fault planes solutions obtained for the 6 Sep 2004 earthquake using the RMT technique at a fixed depth of 10 km compared with the HRV	

moment tensor solution. Synthetic (red line) and observed (blue line) records are shown given for each component (vertical, radial and tangential). The station code, the distance from the source to the station in kilometers and the azimuth from the source to the station are shown above the waveforms.	31
Figure 12: Source mechanism, magnitude and fault planes solutions obtained for the 11 Dec 2004 earthquake using the RMT technique at a fixed depth of 10 km compared with the HRV moment tensor solution. Synthetic (red line) and observed (blue line) records are shown given for each component (vertical, radial and tangential). The station code, the distance from the source to the station in kilometers and the azimuth from the source to the station are shown above the waveforms.	32
Figure 13: Source mechanism, magnitude and fault planes solutions obtained for the 18 Dec 2004 earthquake using the RMT technique at a fixed depth of 10 km compared with the HRV moment tensor solution. Synthetic (red line) and observed (blue line) records are shown given for each component (vertical, radial and tangential). The station code, the distance from the source to the station in kilometers and the azimuth from the source to the station are shown above the waveforms.	33
Figure 14: Source mechanism, magnitude and fault planes solutions obtained for the 14 Feb 2005 earthquake using the RMT technique at a fixed depth of 10 km compared with the HRV moment tensor solution. Synthetic (red line) and observed (blue line) records are shown given for each component (vertical, radial and tangential). The station code, the distance from the source to the station in kilometers and the azimuth from the source to the station are shown above the waveforms.	34
Figure 15: Source mechanism, magnitude and fault planes solutions obtained for the 2 Mar 2006 earthquake using the RMT technique at a fixed depth of 10 km compared with the HRV moment tensor solution. Synthetic (red line) and observed (blue line) records are shown given for each component (vertical, radial and tangential). The station code, the distance from the source to the station in kilometers and the azimuth from the source to the station are shown above the waveforms.	35
Figure 16: (A) New high-resolution multibeam bathymetric survey of the Puerto Rico Trench (modified after ten Brink and Lin, 2004), showing active fault geometry of the Puerto Rico and U.S. Virgin Islands forearc and RMT focal mechanisms. (B) Low-resolution Smith and Sandwell (1997) Satellite Altimetry bathymetry data showing the same area coverage as the new high-resolution multibeam bathymetric survey, also showing the RMT focal mechanism. RMT focal mechanism show thrust or left lateral strike-slip motion along this plate margin, consistent with the known geology.....	36

1 INTRODUCTION

This thesis presents the results of the application of a regional moment tensor inversion procedure to regional earthquakes within the eastern part of the Caribbean to provide a complete description of the size, depth, and faulting geometry. This work initially describes the seismotectonic setting of the eastern Caribbean region and then shifts its attention to the Puerto Rico-Virgin Islands (PRVI) region. Next, this investigation addresses the lack of local capabilities (PRSN) to extract information about the earthquake source, in particular, seismic moment, focal mechanisms, and centroid depth to be used as an initial indication of the potential of tsunami generation in the region.

1.1 Eastern Caribbean Seismotectonic Setting and Tsunami History

Large and frequent earthquakes characterize the eastern Caribbean region. Figure 1 shows earthquakes with magnitudes greater than 5.0 catalogued by the U. S. National Earthquake Information Center (NEIC) since 1900. The distribution of earthquakes within 1° to 12° epicentral distance from PRSN stations can be divided into several sub-regions or zones. These have been identified on the basis of their geologic characteristics as well as their seismicity. These sub-regions or zones are detailed on Figure 2 and a brief description follows:

- a. Northern Caribbean Plate Boundary Zone (Eastern Hispaniola) - the North America- Caribbean plate boundary zone consists of a 100- to 250- km wide seismogenic zone of mainly left-lateral strike-slip deformation extending over 2,000- km along the northern edge of the Caribbean Sea (Dolan and Mann, 1998).

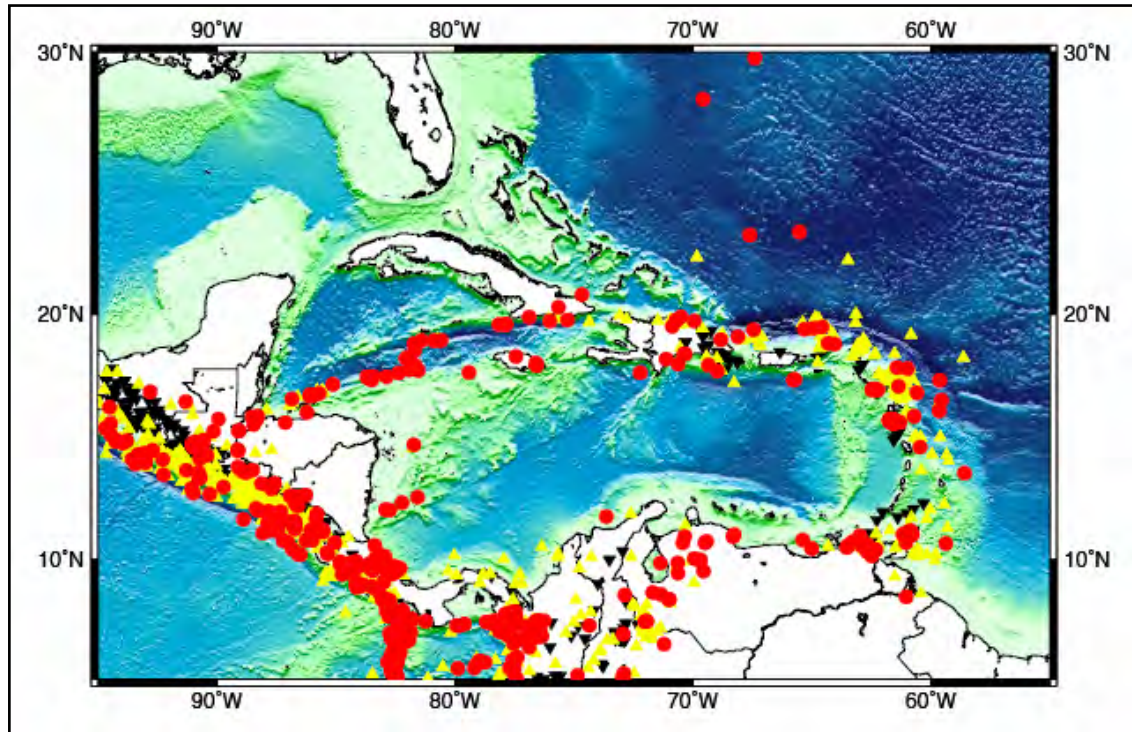


Figure 1: Map of the Circum-Caribbean region seismicity. Epicenters are for earthquakes with magnitudes >5 with focal depth shallower than 30 km (red dots), between 30- to 70- km (yellow triangles) and deeper than 70 km (inverted black triangles) from 1 January 1973 until 31 December 2005 (National Earthquake Information Center).

- b. Mona Canyon - is located between Dominican Republic and Puerto Rico, and is bounded by seismogenic fault zones. The Mona Canyon was the focus of one of the most destructive tsunanigenic - earthquakes in the Puerto Rico region, the October 11, 1918, earthquake. Studies of the seafloor structure suggest an E-W extension occurring in this region (Larue and Ryan, 1990; Jansma et al., 2000).
- c. Lesser Antilles Subduction Zone - the 850- km-long Lesser Antilles island arc forms the eastern boundary of the Caribbean plate beneath which the Atlantic crust is subducted (Christeson et. al., 2003). GPS geodetic data indicates that the North America plate is subducting beneath the Caribbean plate at a rate of 2.1 cm/yr oriented along 247° (DeMets et. al., 2000).

- d. Cuba Oriente Fault Zone (OFZ) - is located along the southeastern Cuban margin, it marks the boundary between the North American and Caribbean Plates between Cuba and Hispaniola. Strike-slip deformation dominates, it extends 900- km from the Cayman Spreading Center (CSC) to the Dominican Republic (Moreno, 2002).
- e. Northeastern Puerto Rico (Sombrero Seismic Zone) - the Sombrero Seismic Zone (SSZ) is one of the most active seismic zones in the region. All earthquakes that occur within this zone share similar characteristics; they are usually shallow at 25- km or less and have similar magnitudes (3.0-4.5) (PRSN, 2006). According to reports issued by the PRSN the SSZ is located between the 18.5-19.0-north latitude.
- f. Anegada Passage - the Anegada Passage connects the Neogene Virgin Islands and Witting basins in the southwest with the Sombrero basin in the northeast and defines a zone of probable transtension along which a displacement from the eastern end of the Muertos Trough is transferred to the Puerto Rico trench (Jany et al., 1987; Masson and Scanlon, 1991).
- g. Muertos Trough - extends for about 650- miles parallel to the Greater Antilles, south of Puerto Rico. It is a broad gentle depression dipping to the north. The zone is basically aseismic. It has been suggested that the Puerto Rico-Virgin Islands (PRVI) microplate crust is overriding the Caribbean lithosphere at the western part of the microplate (Ladd et al., 1977; Byrne, et al., 1985). A new multibeam high-resolution bathymetry digital model of the seafloor south of southeastern Hispaniola and southwestern Puerto Rico provides observations that

are consistent with an overriding Caribbean lithosphere by southwestern Puerto Rico along the Muertos Trough (Carbó, et. al., 2005).

- h. Northern Venezuela (Pilar-Bonocó Fault Zone) - the Pilar-Bonocó fault is an active, Late Pleistocene-Holocene fault system, which extends for over 1300- km between the Venezuela-Colombia border, through the Venezuela Andes and along the northern Venezuela coast, to the east of Trinidad (Schubert, 1984).

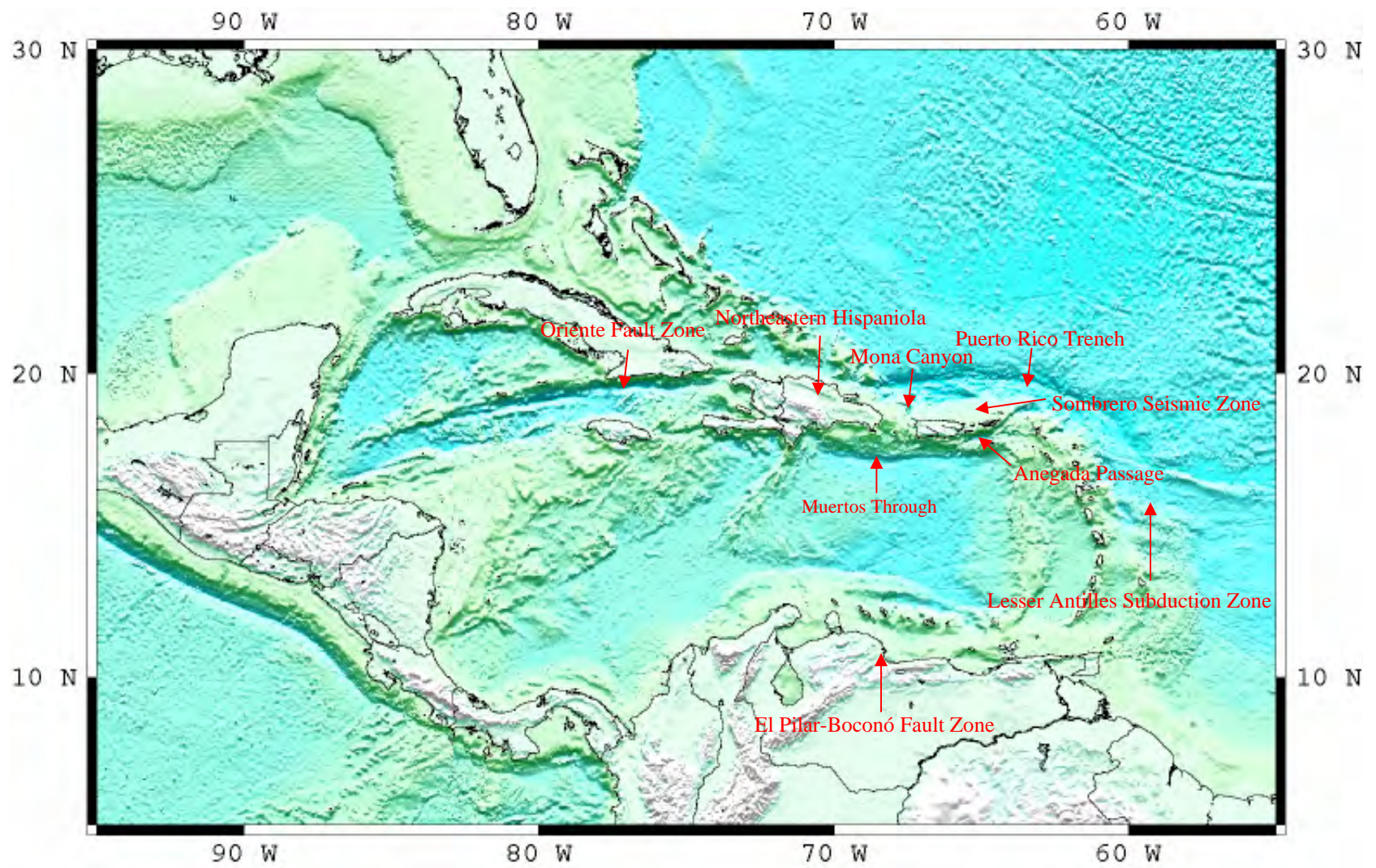


Figure 2: Seismo-Tectonic zones in the eastern Caribbean.

Lander et al., (2002) have catalogued the historical tsunamis in the Circum-Caribbean since 1530 (Figure 3). Of the 35 tsunamis catalogued by Lander et al., (2002) 16 of those have occurred since 1900. Tsunamis since 1900 in the Circum-Caribbean are also shown in figure 3.

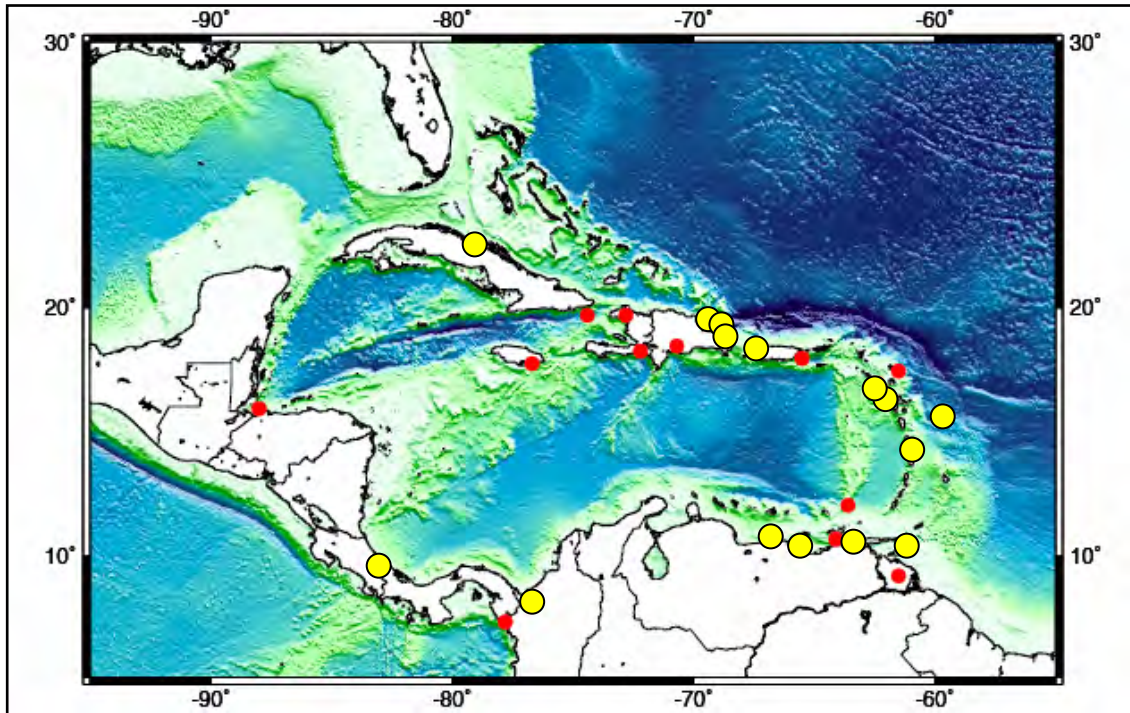


Figure 3: Tsunamis in the Caribbean region 1530-1997 (red and yellow dots). Yellow dots represent tsunamis from 1900-1997 (after Lander et al., 2002).

1.2 Puerto Rico-Virgin Islands

Puerto Rico and the Virgin Islands (PRVI) are characterized by large, infrequent, damaging earthquakes, located within the highly oblique oceanic subduction-strike-slip transition area along the North America-Caribbean plate boundary (Figure 4). Historically, several large damaging earthquakes have occurred in the region, including the April 24, 1916 ($M_s = 7.2$), October 11, 1918 ($M_s = 7.3$), and the July 29, 1943 ($M_s = 7.5$) Mona Passage earthquakes; the

November 18, 1867 ($M_s = 7.3$) Anegada earthquake and the May 2, 1787 ($M = 7.5?$) Puerto Rico Trench earthquake (Figure 4), (Pacheco and Sykes, 1992).

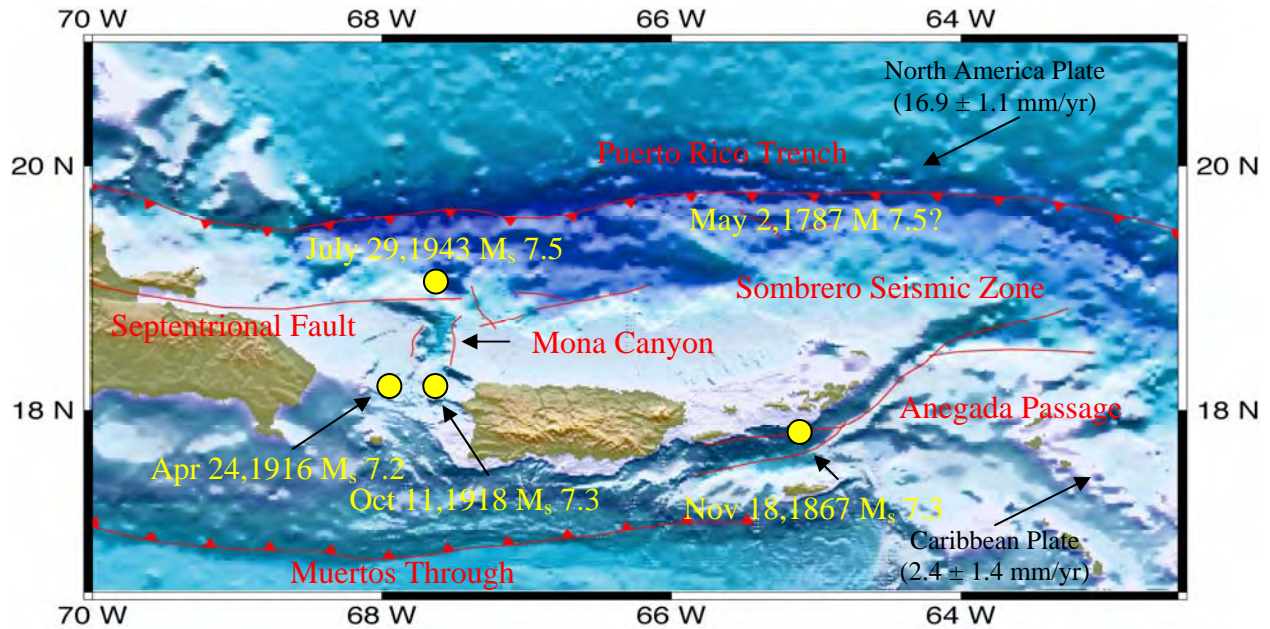


Figure 4: Bathymetric and tectonic map of the Puerto Rico, Virgin Islands, and eastern Hispaniola area showing the seismo-tectonic structures in the PRVI region. Yellow dots represent several damaging earthquakes in the PRVI region (Pacheco and Sykes, 1992). Vectors represent the relative plate motion and the plate speeds were taken from Jansma et al., (2000).

The 1867 and 1918 earthquakes generated tsunamis. The tsunami of November 18, 1867 was triggered by an $M_s = 7.3$ earthquake. This tsunami generated 6-meter waves in Charlotte Amalie, St. Thomas and 9.0-meter waves in Fredricksted, St. Croix. The tsunami had a run-up of 6-meters in southeastern Puerto Rico and almost 20-meters in Guadeloupe (Lander et al., 2002). A total of 17 people drowned in the U.S. Virgin Islands and 23 deaths were reported in Guadeloupe; no deaths were reported in Puerto Rico.

On October 11, 1918 an earthquake of $M_s = 7.3$ occurred in the Mona Canyon, 40- km WNW of Aguadilla, Puerto Rico, generating a tsunami. According to Reid and Taber (1919) the

water was observed to recede within a minute of the earthquake itself along the westernmost point of Puerto Rico. Wave heights of up to 6-meters were observed in western Puerto Rico. It is important to point out that these two earthquakes (1867, 1918) and tsunamis were not generated within the highly oblique oceanic subduction-strike-slip transition area along the North America-Caribbean plate boundary. New GPS derived velocities from Hispaniola and the Puerto Rico-Virgin Islands platform yield east-west extension across the N-S Mona Canyon (Jansma, et al., 2000, 2005).

Moya and Mercado (2004) documented 3 tsunami deposits in northwestern Puerto Rico, one of which corresponds to the 1918 event and the other two were dated at 1270 – 1410 AD and 820 – 400 BC. The source of these tsunami deposits is uncertain but reinforces the idea that tsunamis have been a recurrent phenomenon, suggesting that low lying coastal areas of the PRVI region can be impacted by tsunamis in any time.

1.3 Problem Statement and Objectives

Warning centers have been established in other areas of the world to alert of impending tsunamis (e.g., west coast of the United States, Alaska and the Pacific region). The Pacific Tsunami Warning Center (PTWC) in Ewa Beach, Hawaii, provides warnings for teletsunamis in most countries in the Pacific Basin as well as in Hawaii and all other US interests in the Pacific outside of Alaska and the US West Coast. The West Coast & Alaska Tsunami Warning Center (WC/ATWC) in Palmer, Alaska, serves as the regional Tsunami Warning Center for Alaska, British Columbia, Washington, Oregon, and California. The objective of the PTWC as well as

WC/ATWC is to detect, locate, and determine the magnitude of potentially tsunamigenic earthquakes occurring in the Pacific Basin or its immediate margins. If the location and magnitude of an earthquake meet a pre-set criterion (e.g., size and centroid depth) for generation of a tsunami, a tsunami warning is issued to warn of an imminent tsunami hazard. However, the northeastern Caribbean region lacks the capabilities to extract information about the earthquake source, in particular, seismic moment, focal mechanisms, and centroid depth to be used as an initial indication of the potential of tsunami generation (von Hillebrandt and Huérfano, 2005).

The main objectives of this investigation were:

- To apply a regional moment tensor (RMT) inversion scheme to regional waveforms (regional earthquakes) recorded by the PRSN and illustrate the capabilities of this network to model regional seismic activity.
- To examine the ability of the RMT scheme to provide quantitative information about regional earthquakes (centroid depth, size and fault parameters) for earthquakes located in the eastern part of the Caribbean.
- To aid with the identification of potentially-tsunamigenic events in the eastern Caribbean.

2 DATA AND METHODOLOGY

2.1 Data

Our analysis is based on recordings of regional waveforms recorded by the PRSN for six events during 2003-2006 (Table 2.1-1). These events were used because they met the following conditions: (1) they were located within 1° to 12° epicentral distance from the PRSN stations; (2) the events had a local magnitude of 4.5 or greater; (3) they were recorded by at least one PRSN broadband station; and (4) they were recorded by a minimum of ~ 200 sec before and after the P-wave arrival (Appendix A).

Table 2.1-1: PRSN – List of events used in this study.

Event	Time GMT	Lat ($^{\circ}$)	Lon ($^{\circ}$)	Depth (km)	Magnitude	Region
09/22/2003	04:45:20.99	19.9	-70.61	9.8	6.5	Dominican Republic
09/06/2004	20:43:03.52	19.48	-65.5	25.2	5.3	Puerto Rico Trench
12/11/2004	19:45:47.14	18.76	-64.69	24.8	4.5	Virgin Islands
12/18/2004	00:35:32.50	19.17	-64.75	35.7	4.7	Virgin Islands
02/14/2005	18:06:03.02	15.91	-61.57	25.0	6.1	Leeward Islands
03/02/2006	23:35:44.35	19.17	-63.95	24.8	5.3	Virgin Islands

The PRSN operates 23 digital seismographs that record local, regional and teleseismic events. A list of the PRSN broadband stations, type of instrument and the instrument response bandpass are shown in Table 2.1-2. In this work, only those stations with CMG-3T and CMG-3ESP instruments were used (Figure 5). Mendoza and Huérfano, (Personal Communication) tested the instrument responses for the -3T and -3ESP instruments (Appendix B) by comparing the deconvolved vertical ground velocities observed at each site for the Mw 8.7 Sumatra event of

March 2005 with the deconvolved vertical ground velocity record from the GSN station SJG (Figure 6). The comparison showed almost identical ground motion both in amplitude and in waveform shape, indicating that at least for these stations (AGPR, AOPR, CBYP, CRPR, HUMP, and MPR) the vertical instrument response appears to be correct. No information was available for the horizontal components.

Table 2.1-2: Seismic stations used in this work.

Station	Location	Network	Lat (°)	Lon (°)	Elevation	Sensor	Flat response	DAS
AGPR	Aguadilla, PR	PR	18.47	- 67.11	119.84 m	CMG-3T	.003 - 360 s	Net-Das
AOPR	Arecibo, PR	PR	18.35	- 66.76	355.15 m	CMG-3T	.003 - 360 s	Net-Das
CBYP	Canovanas, PR	PR	18.27	- 65.86	606.90 m	CMG-3ESP	.01 - 120 s	Ref-Tek
CRPR	Cabo Rojo, PR	PR	18.01	- 67.11	64.88 m	CMG-3ESP	.01 - 120 s	Ref-Tek
HUMP	Humacao, PR	PR	18.14	- 65.85	79.10 m	CMG-3T	.003 - 360 s	Ref-Tek
MPR	Mayagüez, PR	PR	18.21	- 67.14	22.41 m	CMG-3T	.003 - 360 s	Net-Das
SJG	Cayey, PR	IU	18.11	- 66.15	456.88 m	STS-1	.0027 - 360 s	Quanterra

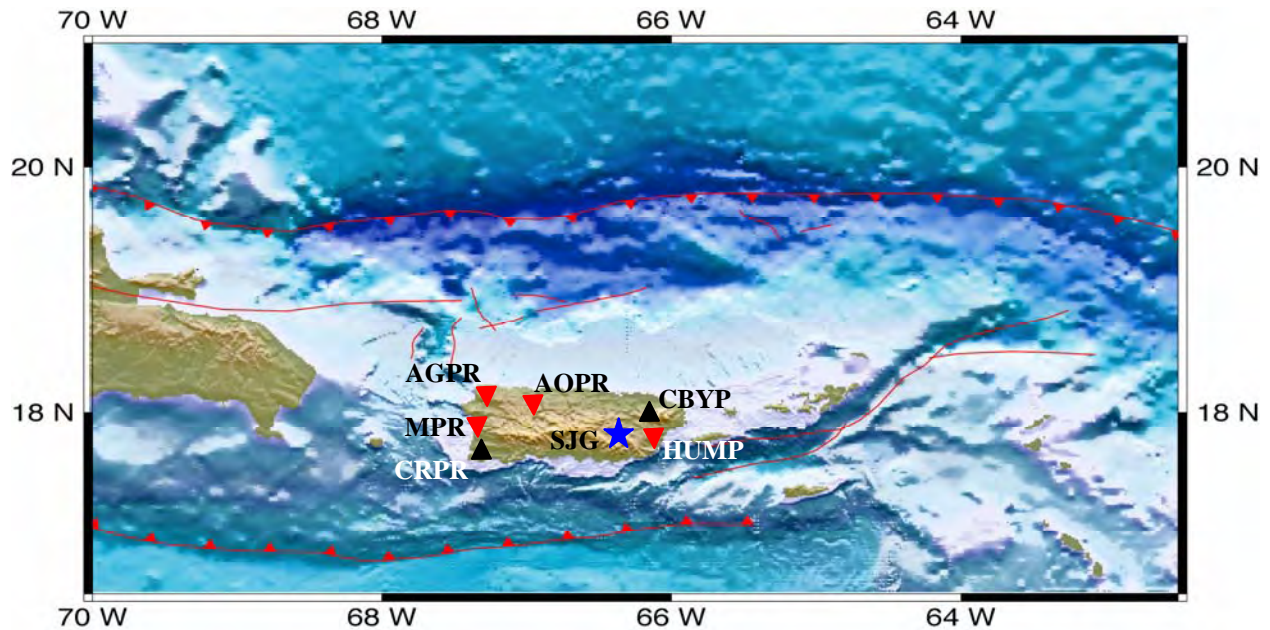


Figure 5: Location map of the PRSN broadband stations used in this study. Inverted red triangles represent realtime CMG-3T sensors. Black triangles are realtime CMG-3ESP sensors; blue star represents a STS-1 sensor that belongs to the Global Seismic Network (GSN).

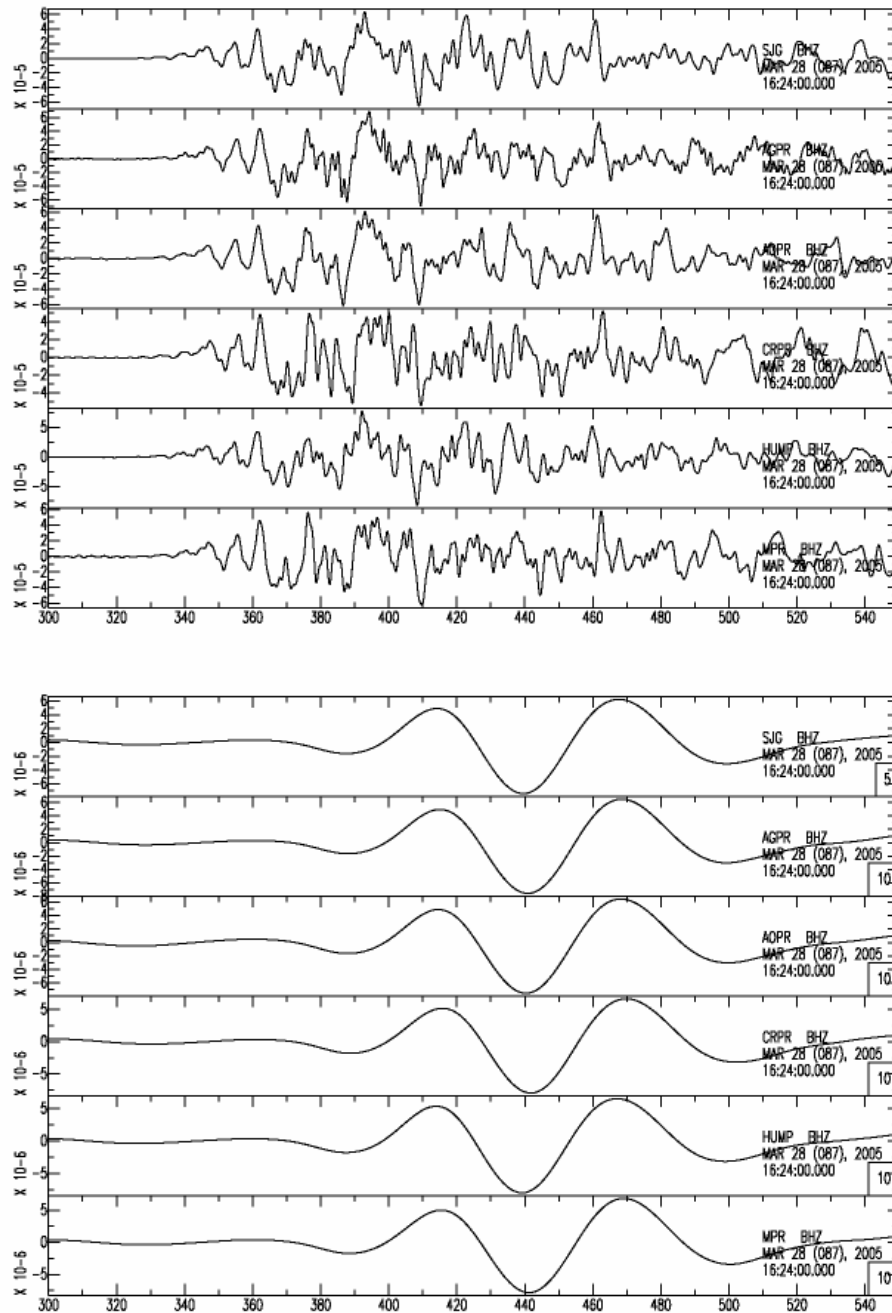


Figure 6: Comparison of the deconvolved vertical ground velocities observed at each PRSN broadband station used in this study for the Mw 8.7 Sumatra event of March 2005 with the deconvolved vertical ground velocity record from the GSN station SJG. (A) Raw deconvolved vertical ground velocities (B) 50- to 100-s bandpass filtered deconvolved vertical ground velocities.

2.2 Waveform Inversion Method

The regional moment tensor (RMT) inversion technique used in this thesis was developed by Randall et al., (1995) and implemented by Mendoza (2005) to estimate the earthquake source mechanism and magnitude from seismic waveforms recorded at regional distances from SJG (Appendix C). The Randall et al., (1995) RMT inversion technique provides the earthquake source mechanism and magnitude for waveforms recorded at regional distances (1° - 12°) of the recording site. The introduction of modern broadband digital regional networks has made it possible to develop moment tensor inversion techniques for smaller magnitude earthquakes at regional distances (Dreger and Helmberger, 1993; Ritsema and Lay, 1993; Romanowicz et al., 1993; Walter 1993; Braunmiller et al., 1995; Nabelek and Xia, 1995; Randall et al., 1995; Thio and Kanamori, 1995; Ammon et al., 1998).

Randall's RMT method uses the time-domain inversion scheme described by Langston (1981) to compute the deviatoric moment tensor from three-component (radial, tangential and vertical) displacement waveforms. Records are modeled at the beginning of the P-wave arrival, and Green's functions are calculated to compute synthetic seismograms using the reflection-matrix method of Kennett (1983) with a step source-time function and an appropriate laterally-homogeneous-crustal velocity model structure. In this study we tested two velocity models: (a) a general regional 15-km thick crustal velocity model obtained from seismic refraction studies in the Caribbean (Ewing et al., 1968) and, (b) the Preliminary Reference Earth Model (PREM); (Dziewonski and Anderson, 1981); (Figure 6) (Appendix D).

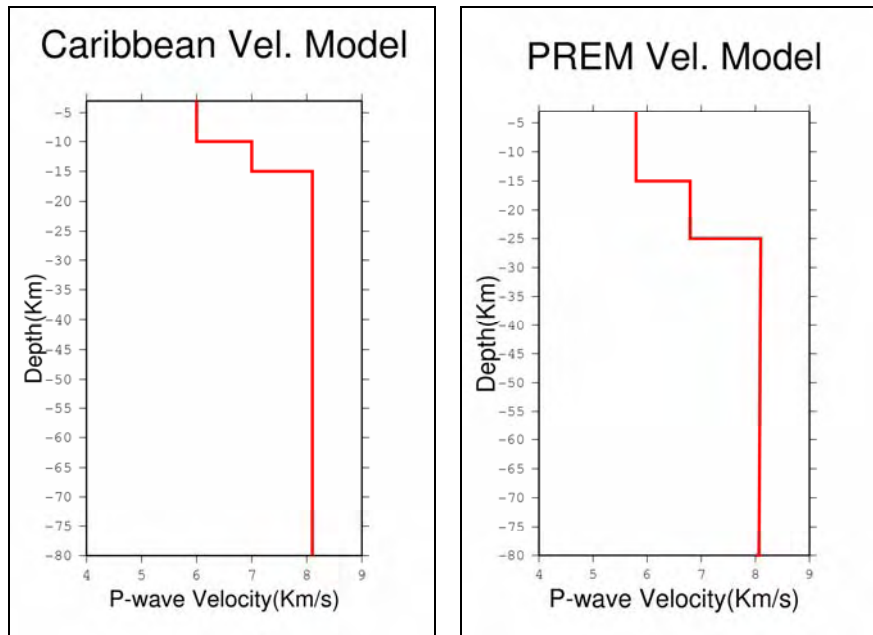


Figure 7: P-wave velocity profile used in this study; (A) the Caribbean velocity model after Ewing et al., (1968) and, (B) the PREM model (Dziewonski and Anderson, 1981).

2.3 Variables Tested and Testing Scheme

In order to implement the RMT technique using the PRSN stations several variables were tested. The variables tested were (not necessarily in this order):

- The velocity model.
- The depth of the event.
- Event Signal-to-Noise.
- Bandpass filter.
- Number of stations.

To test these variables and the relationship between them a testing scheme was designed.

The Testing Scheme basically consists of 4 steps. These are:

Step # 1- Signal-to-Noise Ratio Test – For each station that recorded a regional event, the Signal-to-Noise ratio (SNR) was determined. The SNR was determined in the frequency-domain. The waveform was windowed 200- sec before and after the P-wave arrival. First, we estimated the pre-event noise amplitude spectra, and then we estimated the signal amplitude spectra. Next, both spectra were compared, within the bandpass of the instrument, to determine the SNR. Those events with a $SNR > 2$ were retained for the RMT study.

Step # 2a- Generalized Caribbean Velocity Model (CRB) / fixed depth of 10 Km / filtered with 20- to- 50- sec bandpass filter. Green's functions were estimated using the Generalized CRB velocity model at a fixed depth of 10 km, then the synthetic and observed waveforms were filtered using a 20- to 50- sec bandpass filter. Multi-Station vs. Single-Station inversions were tested. That is: using two or more stations in the inversion procedure (different combinations were used), and Single-Station inversion (different single-stations were used, because not all broadband stations recorded all events).

Step # 2b- PREM Velocity Model / fixed depth of 10 Km / filtered with a 20- to- 50- sec corner bandpass filter. First the Green's functions were estimated using the PREM velocity model at a fixed depth of 10 km, then the synthetic and observed waveforms were filtered using a 20- to 50- sec bandpass filter.

Step # 3a- Generalized Caribbean Velocity Model / fixed depth of 10 Km / filtered with a 30- to- 60- sec bandpass filter. Green's functions were estimated using the generalized CRB velocity

model at a fixed depth of 10 km, then the synthetic and observed waveforms were filtered using a 30- to 60- sec bandpass filter.

Step # 3b- *PREM Velocity Model / fixed depth of 10 Km / filtered with a 30- to- 60- sec bandpass filter.* First the Green's functions were estimated using the PREM velocity model at a fixed depth of 10 km, then the synthetic and observed waveforms were filtered using a 30- to 60- sec bandpass filter.

Step # 4- *Depth Determination.* To estimate the source depth, we implemented an iterative search method. For testing scheme Steps 2a and Step 3a, the depth of the event was changed from 0- to 16- km, at intervals of 2- km. For each testing scheme step 2b and 3b, the depth of the event was changed from 0- to 24- km, at 2- km increments. The depth that produced the minimum error was interpreted to be the centroid depth.

3 RESULTS

3.1 Testing Scheme Results

The variables listed in Section 2.3 and the relationships between them were tested using the Testing Scheme described in Section 2.3. The Results of the Testing Scheme are shown in Tables 3.1.1-1 through 3.1.1-6. These are expressed in terms of root-mean-square errors (RMS), which are calculated by comparing the filtered synthetic with the filtered observed waveforms.

RMS is given by:

$$\frac{1}{npts} \sum_{i=1}^{npts} [Obs(i) - Teo(i)]^2$$

Where:

Obs	Observed waveform
Teo	Synthetic waveform
npts	Number of sample points

Results for each step used on the Testing Scheme:

Step # 1- Signal- to- Noise Ratio Test. All events-station pairs that recorded waveforms with an SNR ratio > 2 were retained for the RMT inversion. An example of the SNR analysis is shown in Figure 8 for the 092203 Dominican Republic event recorded at PRSN station MPR. SNR analyses for the other stations and event pairs are shown in Appendix A.

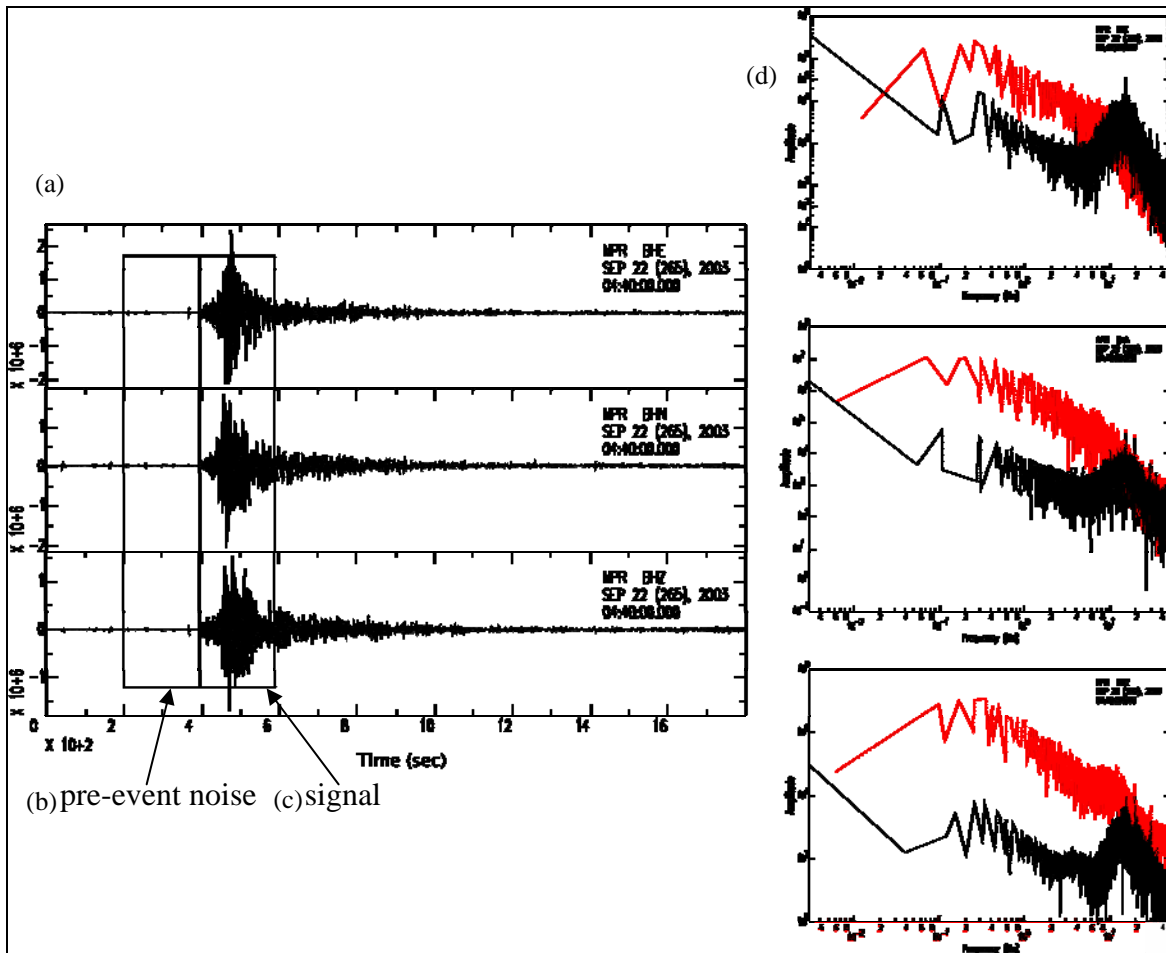


Figure 8: Example of the Signal-to-Noise Ratio analysis for the 092203 Dominican Republic event recorded at PRSN broadband station MPR. Also showing: (a) the 3-component waveforms, (b) the pre-event noise window, (c) the signal window, and (d) the corresponding amplitude spectra, where the signal amplitude spectrum is shown in red, and the pre-event noise amplitude spectrum is shown in black.

Step # 2a- *Generalized CRB velocity model / fixed depth of 10 km / filtered with a 20- to 50- sec bandpass filter.* Results are shown in Tables 3.1-1 through 3.1-6:

- Multi-Station inversion: For all events tested, multi-station inversion had the highest RMS-error. In our testing scheme this was the worst-case scenario.

- Single-Station inversions: For all events tested, the smallest RMS-error was obtained using SJG station alone, with two exceptions. The exceptions were:
 - Station MPR for event 121104, and station AGPR for event 121804.

Step # 2b- *PREM Velocity Model / fixed depth of 10 Km / filtered with a 20- to 50- sec bandpass.* Results are also shown in Tables 3.1-1 through 3.1-6:

- Multi-Station inversion: RMS-errors decrease for all events tested as compared with the Caribbean velocity model.
- Single-Station inversions: For all events tested, the smallest RMS was obtained using station SJG alone. Except in Event 121104 and event 092203 were station MPR had the smallest RMS-error.

Step # 3a- *Generalized CRB velocity model / fixed depth of 10 km / filtered with a 30- to 60- sec bandpass filter.* Results are also shown in Tables 3.1-1 through 3.1-6:

- Multi-Station inversion: in all cases the RMS-errors decrease by using the 30- to 60- sec bandpass corner frequencies as compared to the 20- to 50- sec corner frequencies, with one exception:
 - For event 121104, the filter made no difference.
- Single-Station inversions: Single-Stations inversion RMS-error did not diminish in all cases by changing the filter corner frequencies.

Step # 3b- *PREM Velocity Model / fixed depth of 10 Km / filtered with a 30- to- 60- sec bandpass filter.* Results are also shown in Tables 3.1-1 through 3.1-6:

- Multi-Station inversion: RMS-errors decrease significantly for all events.
- Single-Station inversion: For all events used, the smallest RMS was obtained using SJG-station alone except in Event 121104 and Event 092203 where MPR had the smallest RMS-error. For all events, RMS-errors of individual stations are smaller using the 30- to 60- sec filter, as compared to the 20-to 50- sec filter with the PREM velocity model.

Step # 4- *Depth Determination.* We explore the effects of source depth on the single-station and multi-stations inversions by repeating the RMT analysis for different shallow depths. The iterative search method results are shown in figure 9. We observed that by changing the event depth and repeating the RMT inversion we were not able to constrain the depth of the event.

Table 3.1-1: RMS errors for event 092203 as a function of filter corner frequencies and velocity model. Comparison of three-component (vertical, radial and tangential), broadband displacement waveform data (blue) and synthetics (red) at single-station inversion.

Station	20-50sec./CRB-velocity model/fixed depth		30-60sec./CRB-velocity model/fixed depth		20-50sec./PREM-velocity model/fixed depth		30-60sec./PREM-velocity model/fixed depth	
	RMS	V - R - T	RMS	V - R - T	RMS	V - R - T	RMS	V - R - T
AOPR	.353		.200		.851		.282	
HUMP	.578		.174		.768		.314	
MPR	.691		.737		.141		.069	
SJG	.569		.191		.203		.085	
Multi Stations		.954		.598		.860		.666

Table 3.1-2: RMS errors for event 090604 as a function of filter corner frequencies and velocity model. Comparison of three-component (vertical, radial and tangential), broadband displacement waveform data (blue) and synthetics (red) at single-station inversion.

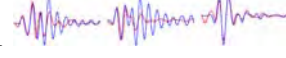
Station	20-50sec./CRB-velocity model/fixed depth		30-60sec./CRB-velocity model/fixed depth		20-50sec./PREM-velocity model/fixed depth		30-60sec./PREM-velocity model/fixed depth	
	RMS	V - R - T	RMS	V - R - T	RMS	V - R - T	RMS	V - R - T
HUMP	.614		.633		.721		.691	
AOPR	.662		.758		.759		.713	
MPR	.787		.217		.64		.080	
AGPR	.895		.685		.701		.517	
SJG	.535		.167		.361		.127	
Multi Stations		.982		.874		.912		.781

Table 3.1-3: RMS errors for event 121104 as a function of filter corner frequencies and velocity model. Comparison of three-component (vertical, radial and tangential), broadband displacement waveform data (blue) and synthetics (red) at single-station inversion.

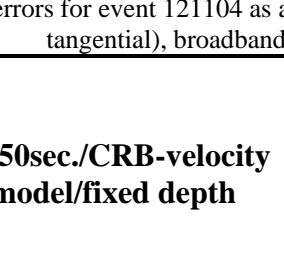
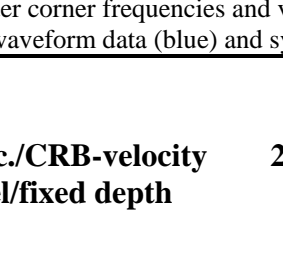
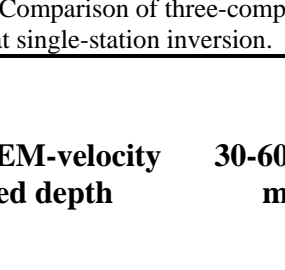
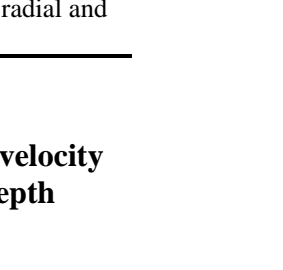
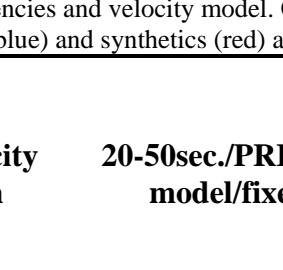
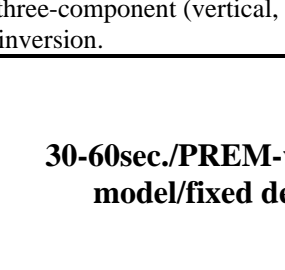
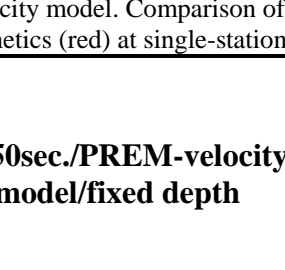
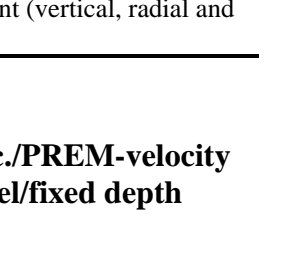
Station	20-50sec./CRB-velocity model/fixed depth		30-60sec./CRB-velocity model/fixed depth		20-50sec./PREM-velocity model/fixed depth		30-60sec./PREM-velocity model/fixed depth	
	RMS	V – R – T	RMS	V – R – T	RMS	V – R – T	RMS	V – R – T
AGPR	.485		.485		.300		.368	
MPR	.379		.379		.355		.243	
SJG	.478		.479		.336		.294	
Multi Stations		.537		.539		.347		.360

Table 3.1-4: RMS errors for event 121804 as a function of filter corner frequencies and velocity model. Comparison of three-component (vertical, radial and tangential), broadband displacement waveform data (blue) and synthetics (red) at single-station inversion.

Station	20-50sec./CRB-velocity model/fixed depth		30-60sec./CRB-velocity model/fixed depth		20-50sec./PREM-velocity model/fixed depth		30-60sec./PREM-velocity model/fixed depth	
	RMS	V - R - T	RMS	V - R - T	RMS	V - R - T	RMS	V - R - T
AOPR	.771		.523		.705		.532	
MPR	.494		.733		.365		.833	
AGPR	.465		.338		.251		.385	
SJG	.534		.304		.100		.258	
Multi Stations		.810		.787		.654		.791

Table 3.1-5: RMS errors for event 021405 as a function of filter corner frequencies and velocity model. Comparison of three-component (vertical, radial and tangential), broadband displacement waveform data (blue) and synthetics (red) at single-station inversion.

Station	20-50sec./CRB-velocity model/fixed depth		30-60sec./CRB-velocity model/fixed depth		20-50sec./PREM-velocity model/fixed depth		30-60sec./PREM-velocity model/fixed depth	
	RMS	V – R – T	RMS	V – R – T	RMS	V – R – T	RMS	V – R – T
AOPR	.900		.219		.224		.178	
AGPR	.869		.196		.378		.248	
SJG	.814		.224		.242		.186	
Multi Stations		.898		.238		.390		.234

Table 3.1-6: RMS errors for event 030206 as a function of filter corner frequencies and velocity model. Comparison of three-component (vertical, radial and tangential), broadband displacement waveform data (blue) and synthetics (red) at single-station inversion.

Station	20-50sec./CAR-velocity model/fixed depth		30-60sec./CAR-velocity model/fixed depth		20-50sec./PREM-velocity model/fixed depth		30-60sec./PREM-velocity model/fixed depth	
	RMS	V - R - T	RMS	V - R - T	RMS	V - R - T	RMS	V - R - T
CBYP	.832		.495		.708		.381	
CRPR	.506		.373		.432		.305	
SJG	.337		.324		.172		.069	
HUMP	.819		.767		.644		.610	
Multi Stations		1		.797		.862		.730

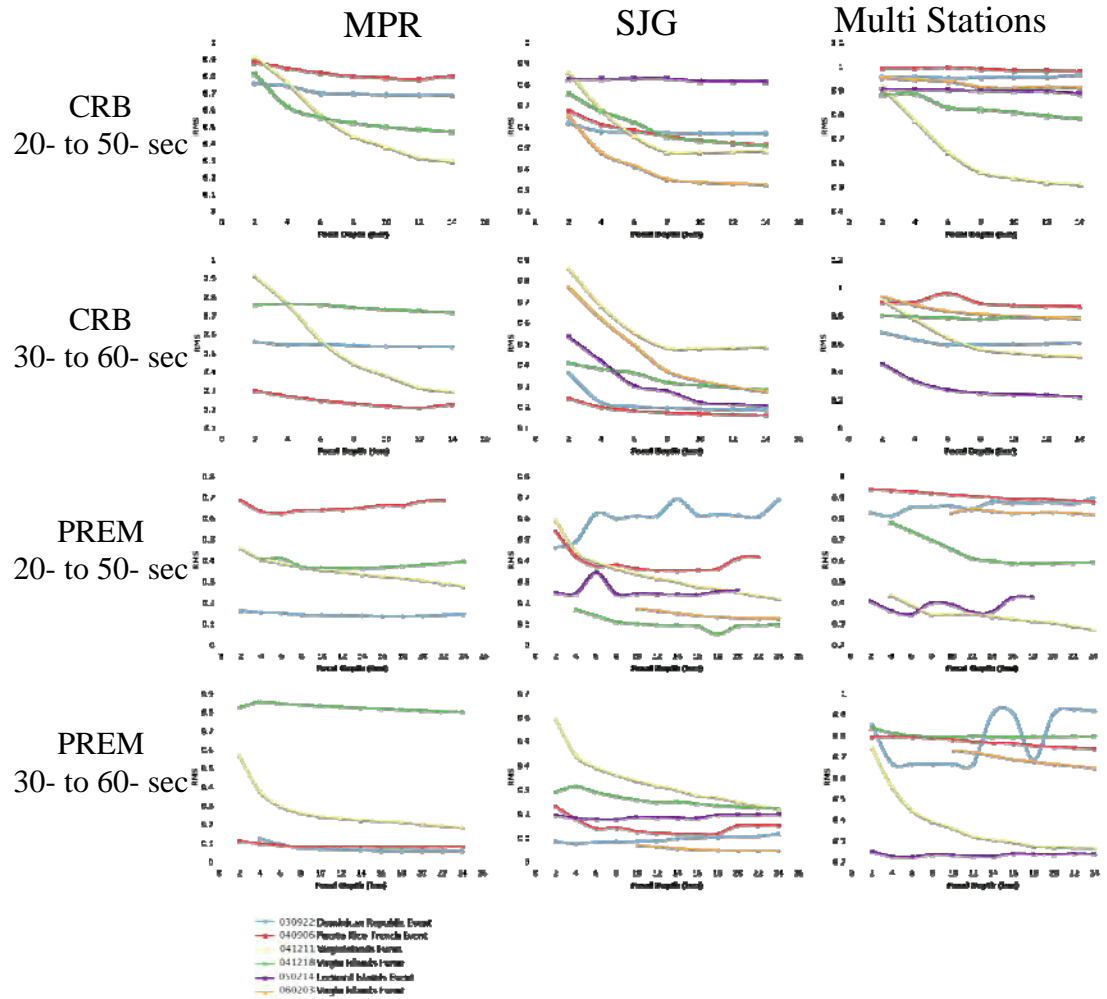


Figure 9: Source-depth analysis for our database. Velocity model as well the passband corner frequencies used are shown to the left of each row. Each column represents an example of hypocentral depth values for single and multi stations.

3.2 RMT Results as Compared to Harvard Centroid Moment Tensor Solutions and the Known Geology of the Area

Focal mechanisms, moment magnitudes and predicted waveforms obtained from the RMT inversions are shown in 10 to 15 (for selected events) together with the corresponding solutions obtained by Harvard University (HRV). The HRV solutions are obtained from a centroid-moment-tensor (CMT) analysis of the globally recorded body- and surfaces-waves (Dziewonski et al., 1981). The RMT and HRV-CMT mechanisms are similar for the 09/22/2003, the 18/12/2004, and the 02/03/2006 earthquakes. Generally some rotation of the principal axes can be seen. These rotations are most severe for the 06/09/2004, the 11/12/2004 and the 12/02/2005 events.

As shown in figures 10 through 15 the RMT inversion technique provides a good first-order constraint of the source parameters as compared to HRV-CMT solutions. Differences between the global and regional results may be due to an incomplete station coverage resulting in the identification of local minima in the inversion (Dreger and Helmberger, 1993) and from uncertainties in earthquake location or from an inexact velocity model. The use of additional stations in the Circum-Caribbean may help constrain the inversion and to identify a more consistent fault mechanism.

All the events used in this study located in the northeastern Caribbean plate margin show thrust or left lateral strike-slip motion. If we compare the strike and dip of the RMT solutions, these appear to tie well (to a first-order constraint) to the known geology of the area. We obtained a copy of the new high-resolution multibeam bathymetric survey of the Puerto Rico

Trench (ten Brink and Lin, 2004) that reveals the active fault geometry of the Puerto Rico and U.S. Virgin Islands forearc. The new sea floor model shows a continuous east-west trending, fresh scarp 10-15 km south of the trench (Figure 16).

We overlaid the RMT-derived focal mechanism over the new high-resolution multibeam bathymetric survey and we observed that wherever the fault was mapped as strike-slip, focal mechanism results are also strike slip likewise, wherever there is a retaining bent in the fault, indicating thrust faulting. We also observed thrust-fault RMT- derived focal mechanisms.

Event	Region	RMT M_w	Fault Planes: Strike, Dip, Rake	RMT Focal Mechanism	Fixed Depth	HRV M_w	Fault Planes: Strike, Dip, Rake	HRV Focal Mechanism	HRV Depth
09/22/2003	Dominican Republic Lon -70.61 Lat 19.90	6.5	P ₁ : 103, 19, 72 P ₂ : 301, 72, 96		10 km	6.4	P ₁ : 110, 10, 85 P ₂ : 295, 80, 91		15 km

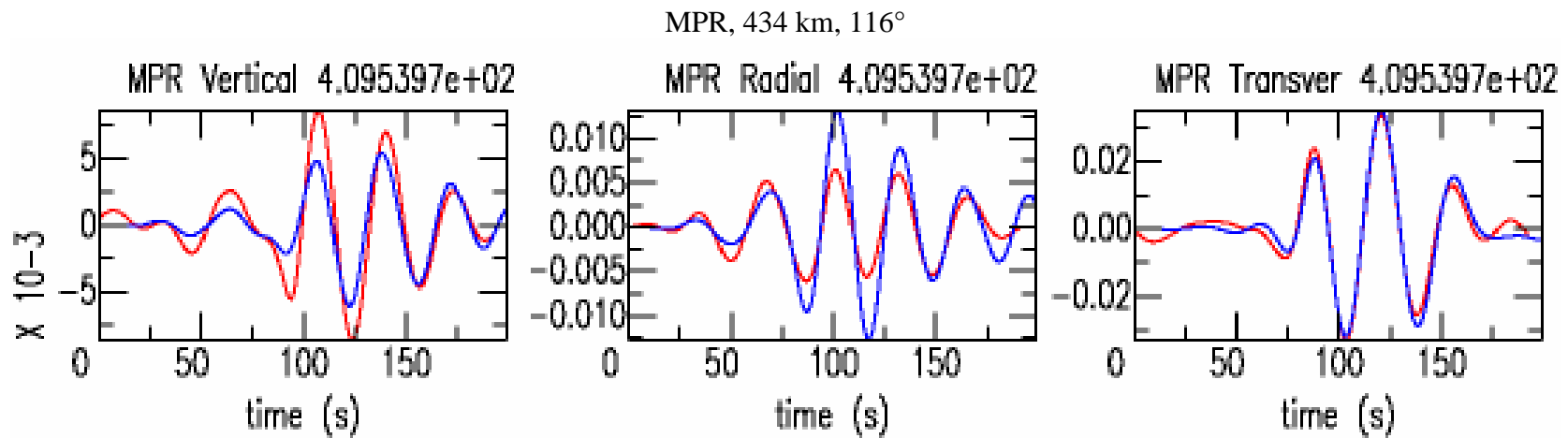


Figure 10: Source mechanism, magnitude and fault planes solutions obtained for the 22 Sep 2003 earthquake using the RMT technique at a fixed depth of 10 km compared with the HRV-CMT moment tensor solution. Synthetic (red line) and observed (blue line) records are shown given for each component (vertical, radial and tangential). The station code, the distance from the source to the station in kilometers and the azimuth from the source to the station are shown above the waveforms.

Event	Region	RMT M_w	Fault Planes: Strike, Dip, Rake	RMT Focal Mechanism	Fixed Depth	HRV M_w	Fault Planes: Strike, Dip, Rake	HRV Focal Mechanism	HRV Depth
09/06/2004	Puerto Rico Trench Lon -65.5 Lat 19.48	5.0	P ₁ : 197, 85, 190 P ₂ : 106, 80, -5		10 km	5.0	P ₁ : 350, 33, 126 P ₂ : 130, 64, 70		16.9 km

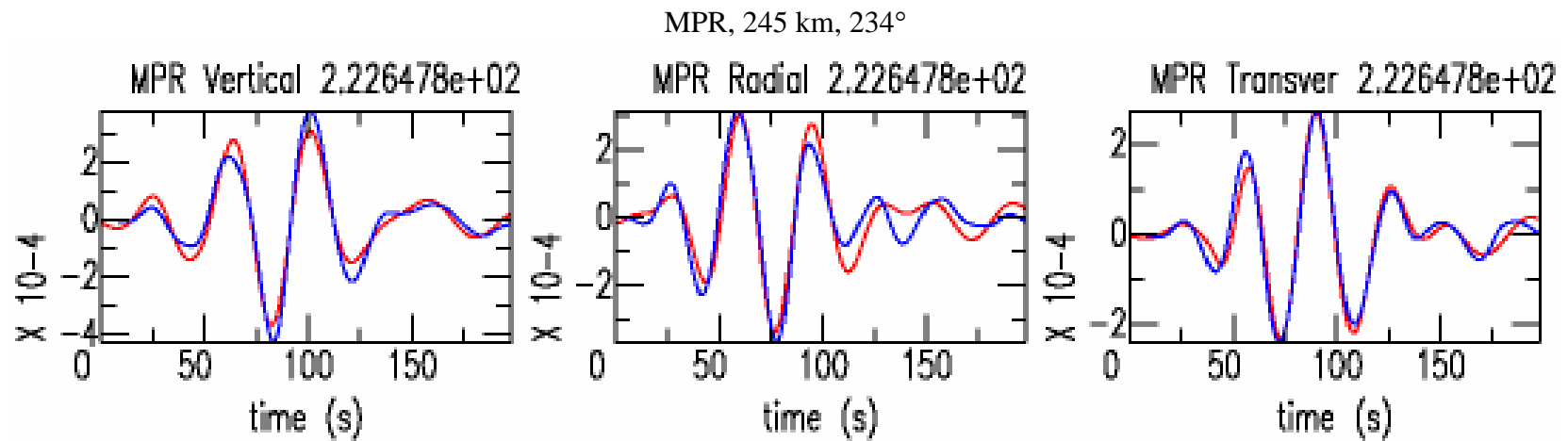


Figure 11: Source mechanism, magnitude and fault planes solutions obtained for the 6 Sep 2004 earthquake using the RMT technique at a fixed depth of 10 km compared with the HRV-CMT moment tensor solution. Synthetic (red line) and observed (blue line) records are shown given for each component (vertical, radial and tangential). The station code, the distance from the source to the station in kilometers and the azimuth from the source to the station are shown above the waveforms.

Event	Region	RMT M_w	Fault Planes: Strike, Dip, Rake	RMT Focal Mechanism	Fixed Depth	HRV M_w	Fault Planes: Strike, Dip, Rake	HRV Focal Mechanism	HRV Depth
12/11/2004	Virgin Islands Lon -64.69 Lat 18.76	5.4	P ₁ : 100, 63, -56 P ₂ : 224, 42, 222		10 km	5.2	P ₁ : 87, 47, 24 P ₂ : 340, 73, 134		48.3 km

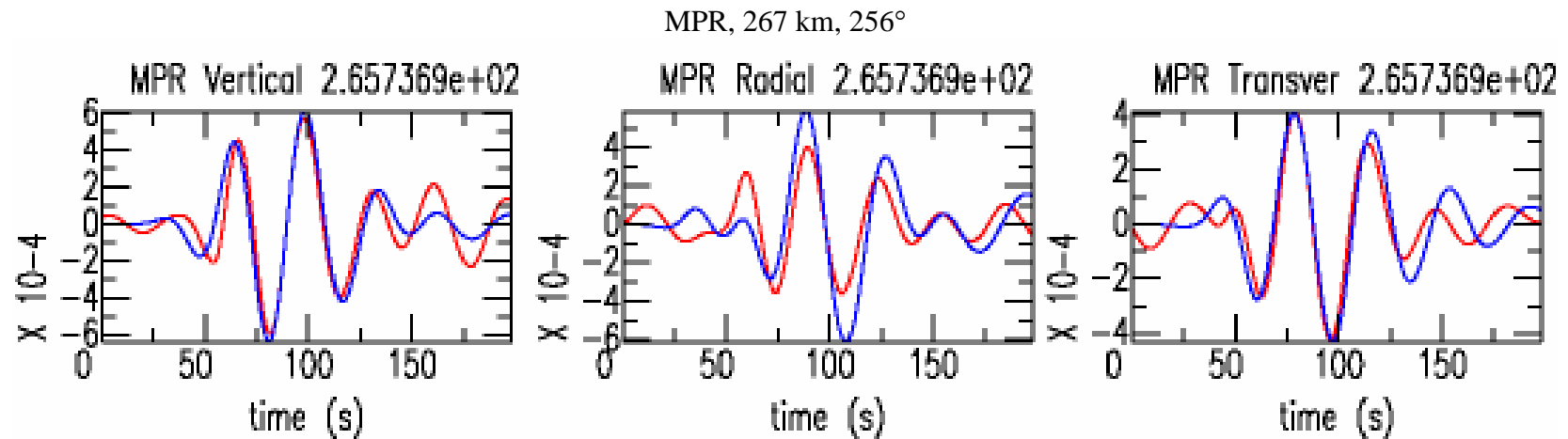


Figure 12: Source mechanism, magnitude and fault planes solutions obtained for the 11 Dec 2004 earthquake using the RMT technique at a fixed depth of 10 km compared with the HRV-CMT moment tensor solution. Synthetic (red line) and observed (blue line) records are shown given for each component (vertical, radial and tangential). The station code, the distance from the source to the station in kilometers and the azimuth from the source to the station are shown above the waveforms.

Event	Region	RMT M_w	Fault Planes: Strike, Dip, Rake	RMT Focal Mechanism	Fixed Depth	HRV M_w	Fault Planes: Strike, Dip, Rake	HRV Focal Mechanism	HRV Depth
12/18/2004	Virgin Islands Lon -64.75 Lat 19.17	4.5	P ₁ : 321, 29, 159 P ₂ : 69, 80, 63		10 km	4.8	P ₁ : 319, 42, 115 P ₂ : 107, 53, 70		36.8 km

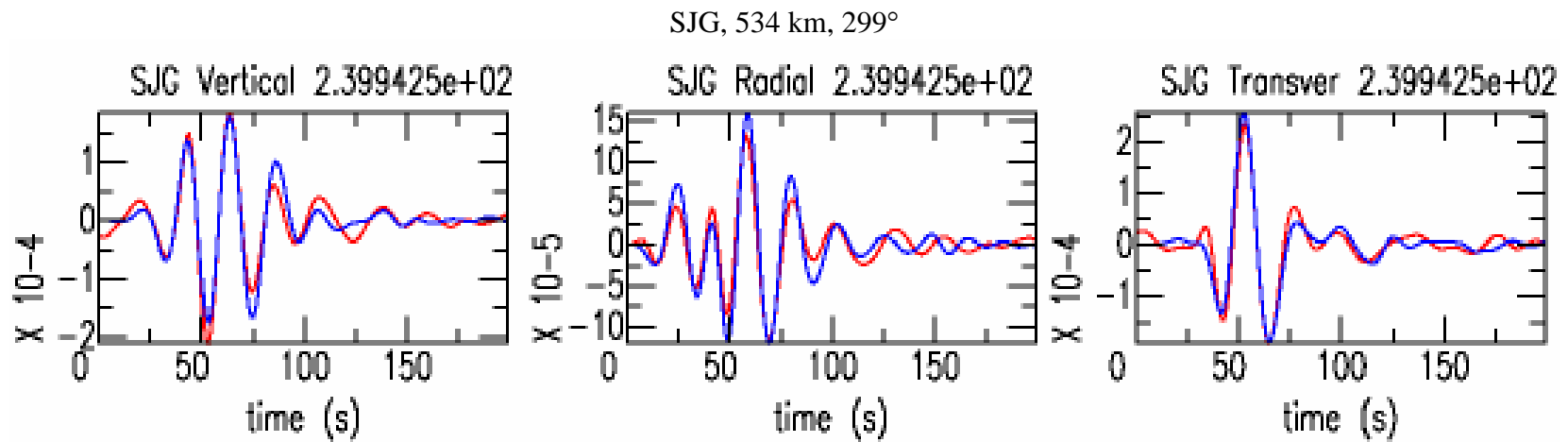


Figure 13: Source mechanism, magnitude and fault planes solutions obtained for the 18 Dec 2004 earthquake using the RMT technique at a fixed depth of 10 km compared with the HRV-CMT moment tensor solution. Synthetic (red line) and observed (blue line) records are shown given for each component (vertical, radial and tangential). The station code, the distance from the source to the station in kilometers and the azimuth from the source to the station are shown above the waveforms.

Event	Region	RMT M_w	Fault Planes: Strike, Dip, Rake	RMT Focal Mechanism	Fixed Depth	HRV M_w	Fault Planes: Strike, Dip, Rake	HRV Focal Mechanism	HRV Depth
02/14/2005	Leeward Islands Lon -61.57 Lat 15.91	5.8	P ₁ : 73, 34, 9 P ₂ : 335, 85, 123		10 km	5.8	P ₁ : 324, 39, -84 P ₂ : 135, 51, -95		12 km

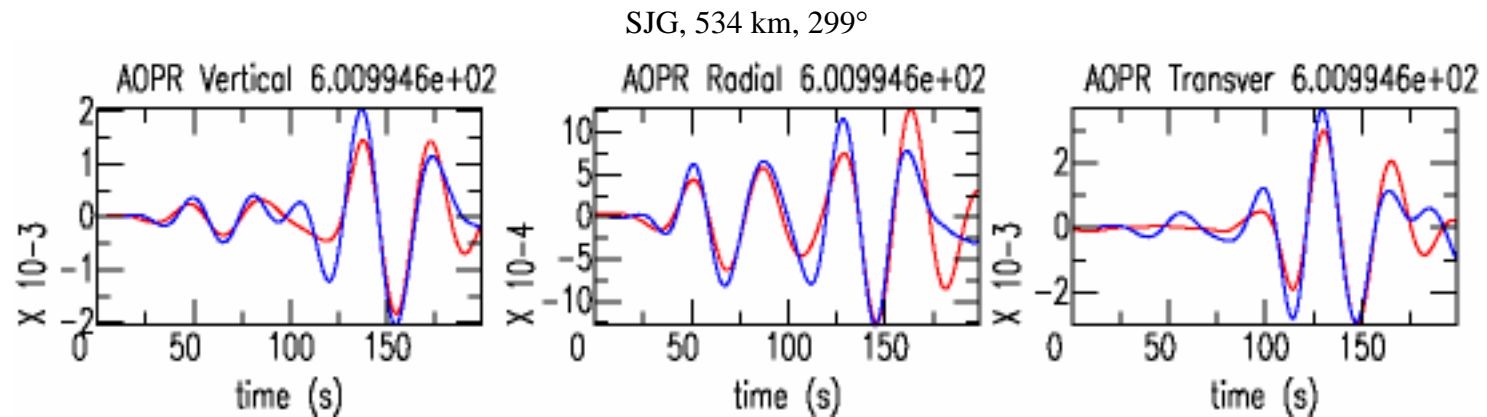


Figure 14: Source mechanism, magnitude and fault planes solutions obtained for the 14 Feb 2005 earthquake using the RMT technique at a fixed depth of 10 km compared with the HRV-CMT moment tensor solution. Synthetic (red line) and observed (blue line) records are shown given for each component (vertical, radial and tangential). The station code, the distance from the source to the station in kilometers and the azimuth from the source to the station are shown above the waveforms.

Event	Region	RMT M_w	Fault Planes: Strike, Dip, Rake	RMT Focal Mechanism	Fixed Depth	HRV M_w	Fault Planes: Strike, Dip, Rake	HRV Focal Mechanism	HRV Depth
03/02/2006	Virgin Islands Lon -63.95 Lat 19.17	5.6	P ₁ : 53, 46, 52 P ₂ : 281, 55, 122		10 km	5.5	P ₁ : 103, 20, 76 P ₂ : 299, 71, 95		15.2 km

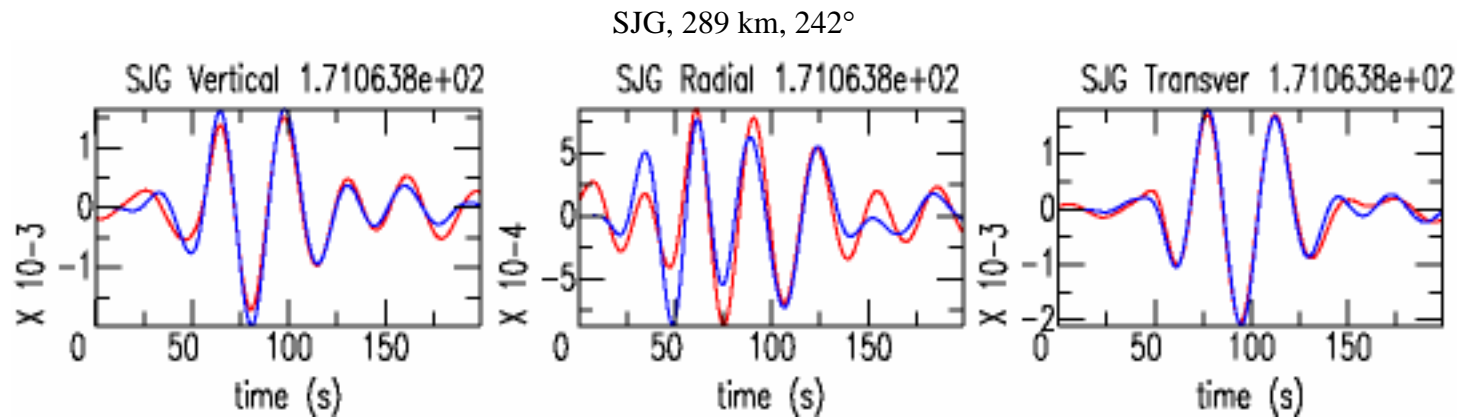
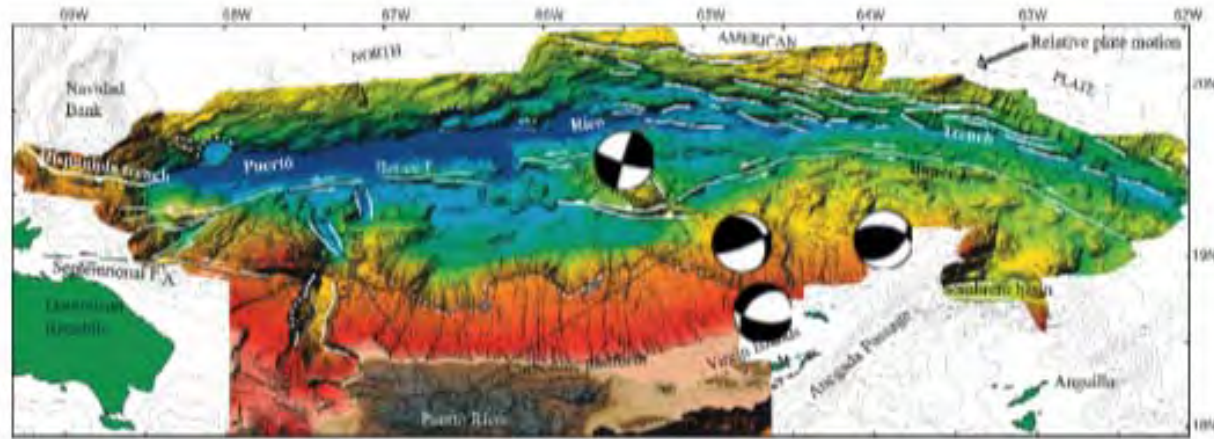


Figure 15: Source mechanism, magnitude and fault planes solutions obtained for the 2 Mar 2006 earthquake using the RMT technique at a fixed depth of 10 km compared with the HRV-CMT moment tensor solution. Synthetic (red line) and observed (blue line) records are shown given for each component (vertical, radial and tangential). The station code, the distance from the source to the station in kilometers and the azimuth from the source to the station are shown above the waveforms.

A



B

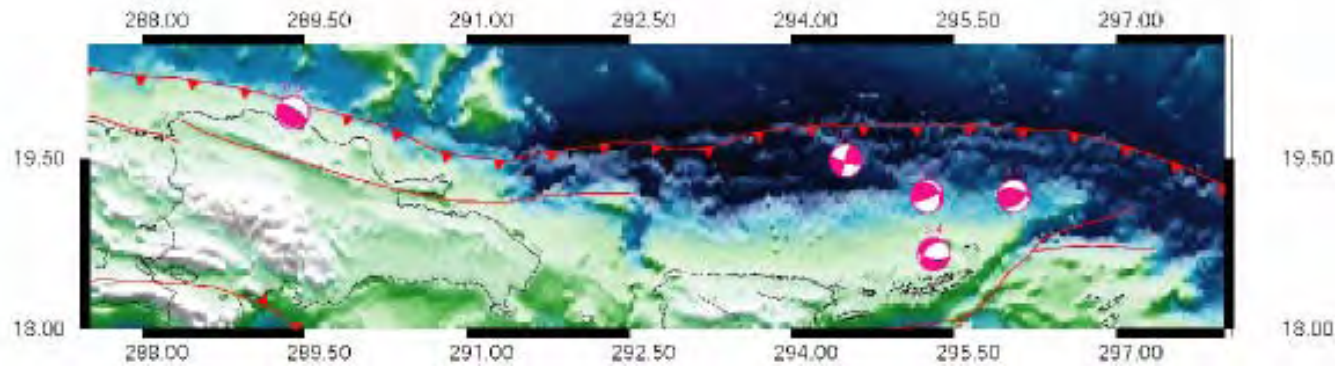


Figure 16: (A) New high-resolution multibeam bathymetric survey of the Puerto Rico Trench (modified after ten Brink and Lin, 2004), showing active fault geometry of the Puerto Rico and U.S. Virgin Islands forearc and RMT focal mechanisms. (B) Low-resolution Smith and Sandwell (1997) Satellite Altimetry bathymetry data showing the same area coverage as the new high-resolution multibeam bathymetric survey, also showing the RMT focal mechanism. RMT focal mechanism show thrust or left lateral strike-slip motion along this plate margin, consistent with the known geology.

4 CONCLUSIONS

As shown in Figures 10 through 15 the RMT inversion technique provides a good first-order constraint of the source parameters as compared to HRV solutions. Differences between the global and regional results may be due to an incomplete station coverage resulting in the identification of local minima in the inversion (Dreger and Helmberger, 1993) and from uncertainties in earthquake location or from an inexact velocity model. The use of additional stations in the Circum-Caribbean may help constrain the inversion and to identify a more consistent fault mechanism.

We also noticed that the RMT technique as adopted by Mendoza (2005) allow us to estimate the moment magnitude of the studied events as accurate as the HRV-CMT.

This thesis evaluated several variables in order to implement the RMT inversion technique using the PRSN dataset for regional events in eastern Caribbean. The variables included: (a) the signal-to-noise-ratio (SNR) of the recorded waveforms, (b) two different bandpass filters with corner frequencies at 20- to 50- sec and 30- to 60- sec., and (c) two velocity models; the regional Caribbean model from Ewing et al., (1968) and the Preliminary Reference Earth Model (PREM) from Dziewonski and Anderson, (1981).

Our results show that using the combination of the PREM velocity model with a 30- to 60- sec bandpass filter with multiple stations improves the RMS, error between the synthetics and observed waveforms. Single PRSN station inversions produce large RMS errors except at SJG and MPR stations. We observed that by changing the event depth and repeating the RMT inversion we were not able to constrain the depth of the event.

5 RECOMENDATIONS

We acknowledge that a detailed analysis of the instrument response wasn't conducted in this study. It is recommended that the vertical and horizontal components of the PRSN broadband stations be conducted and documented.

We also acknowledge that the technique used to constrain the depth of the event did not produce the expected results. This thesis recommends that other techniques should be tested to constrain the depth of the event.

In this study, it was observed that not all broadband stations recorded all the events studied, it is recommended that at the time of implementing these results care should be exercised with the operation of the broadband stations.

The RMT Inversion technique provided a good first-order constraint of the source parameters as compared to HRV solutions Differences between the global and regional results may be due to an incomplete station coverage resulting in the identification of local minima in the inversion (Dreger and Helmberger, 1993) and from uncertainties in earthquake location or from an inexact velocity model. This study recommends to use additional stations in the Circum-Caribbean region (as they become available) to increase the azimuthal coverage used in the inversion procedure. We also recommend to use the tomographic velocity model (like van der Hist, 1991) of the Caribbean to reduce the uncertainties in the velocity model.

REFERENCES

- Ammon, C. J., R. B. Herrmann, C. A. Langston, and H. Benz (1998). Faulting parameters of the January 16, 1994 Wyomissing Hills, Pennsylvania earthquakes, *Seism. Res. Lett.* **69**, 261-269.
- Braunmiller, J., J. Nabelek, B. Leitner, A. Qamar (1995). The 1993 Klamath Falls, Oregon, earthquake sequence: Source mechanism from regional data, *Geophys. Res. Letters*, **22**, 105-108.
- Byrne, D. B., G. Suarez, and W. R. McCann (1985). Muertos Through subduction-Microplate tectonics in the Caribbean, *Nature*, **317**, 420-421.
- Carbó A., D. Córdoba, J. Martín Dávila, U. ten Brink, P. Herranz, C. von Hillebrandt, J. Payero, A. Muñoz Martín, A. Pazos, M. Catalan, J. L. Granja, and M. Gómez, Survey explores active tectonics in northeastern Caribbean, *EOS, Transactions of the American Geophysical Union*, **89**, 537.
- Christeson, G. L., N. L. Bangs, and T. H. Shipley (2003). Deep structure of an island arc backstop, Lesser Antilles subduction zone, *Journal of Geophysical Research*, **108**, doi:10.1029/2002JB002243,2003.
- DeMets, C., P. Jansma, G. Mattioli, T. Dixon, F. Farina, R. Bilham, E. Calais, and P. Mann (2000). GPS geodetic constrain on Caribbean-North America plate motion: Implications for plate rigidity and oblique plate boundary convergence, *Geophys. Res. Letters*, **27**, 437-440.

- Dolan J. F., and P. Mann (1998), Active Strike-Slip and Collisional Tectonics of the Northern Caribbean Plate Boundary Zone, *The Geological Society of America Special Paper*, **326**, p. 174.
- Dreger, D. S., and D. V. Helmberger (1993). Determination of source parameters at regional distances with three components sparse network data, *Geophys. Res. Letters*, **98**, 8107-8125.
- Dziewonski, A. M., and D. L. Anderson (1981). Preliminary reference earth model, *Phys. Earth Planet. Int.*, **25**, 297-356.
- Ewing, J. I., N. T. Edgar, J. W. Antoine (1968). Structure of the Gulf of Mexico and Caribbean Sea, in *The Sea*, A. E. Maxwell and John Wiley (Editors), **4**, part II, New York, 664 pp.
- Jansma, P. E., G. S. Mattioli, A. Lopez, C. DeMets, T. H. Dixon, P. Mann, E. Calais (2000). Neotectonics of Puerto Rico and the Virgin Islands, northeastern Caribbean, from GPS geodesy. *Tectonics*, **19**, 1021-1037.
- Jansma, P. E., and G. S. Mattioli (2005). GPS results from Puerto Rico and the Virgin Islands: Constraint on tectonic setting and rates of active faulting, in *Active tectonics and seismic hazards of Puerto Rico, the Virgin Islands, and offshore areas*, P. Mann (Editor). Geological Society of America Special Paper 385, 13-30.
- Jany, I., K. M. Scanlon, A. Mauffret (1990). Geological interpretation of combined seabeam, gloria, and seismic data from Anegada Passage (Virgin Islands, North Caribbean), *Marine Geophysical Researches*, **12**, 173-196.
- Ladd, J. W., J.L. Worzel, and J. S. Watkins, (1977). Multifold seismic reflection records from the northern Venezuela Basin and the north slope of Muertos trench, in *Island Arcs, deep-sea*

- trenches and back-arc basins*, M. Talwani, and W. C. Pitmann (Editors), American Geophysical Union, 41-56.
- Larue, D. K., and H. F. Ryan (1990). Extensional tectonisms in the Mona Passage, Puerto Rico and Hispaniola: a preliminary studies, *Transactions of Caribbean Geological Conference*, **12**, 301-313.
- Kennett, B. L. N. (1983). *Seismic wave propagation in stratified media*, Cambridge Univ. Press, Cambridge, England, 342 pp.
- Lander, J. F., L. S. Whiteside, P. A. Lockridge (2002). A brief history of tsunamis in the Caribbean Sea, *Science of Tsunami Hazard*, **20**, 57-94.
- Masson, D. G., and K.M. Scanlon (1991). The neotectonics setting of Puerto Rico, *Geological Society of America Bulletin*, **103**, 144-154.
- Mendoza, C. (2005). Earthquake source-parameter estimation using regional waveforms: Implications for tsunami alerting in the Caribbean. *Geophys. Res. Lett.*, **32**, L24314, doi: 10.29/2005GL024435.
- Mendoza, C., and V. Huérfano (2006). Local and regional waveforms analysis for rapid monitoring of shallow Caribbean earthquakes, In *Caribbean Tsunami Hazards, Proceedings of the NSF Caribbean Tsunami Workshop, San Juan, Puerto Rico, 30-31 March 2004* eds. A. Mercado and P. Liu, 96-85.
- Moreno, B. (2002). The new Cuban Seismograph Network, *Seism. Res. Lett.*, **73**, 504-517.
- Moya, J. C., and A. Mercado (2004). Geomorphologic and stratigraphic investigations on historic and prehistoric tsunami in Northwestern Puerto Rico: Implications for long term

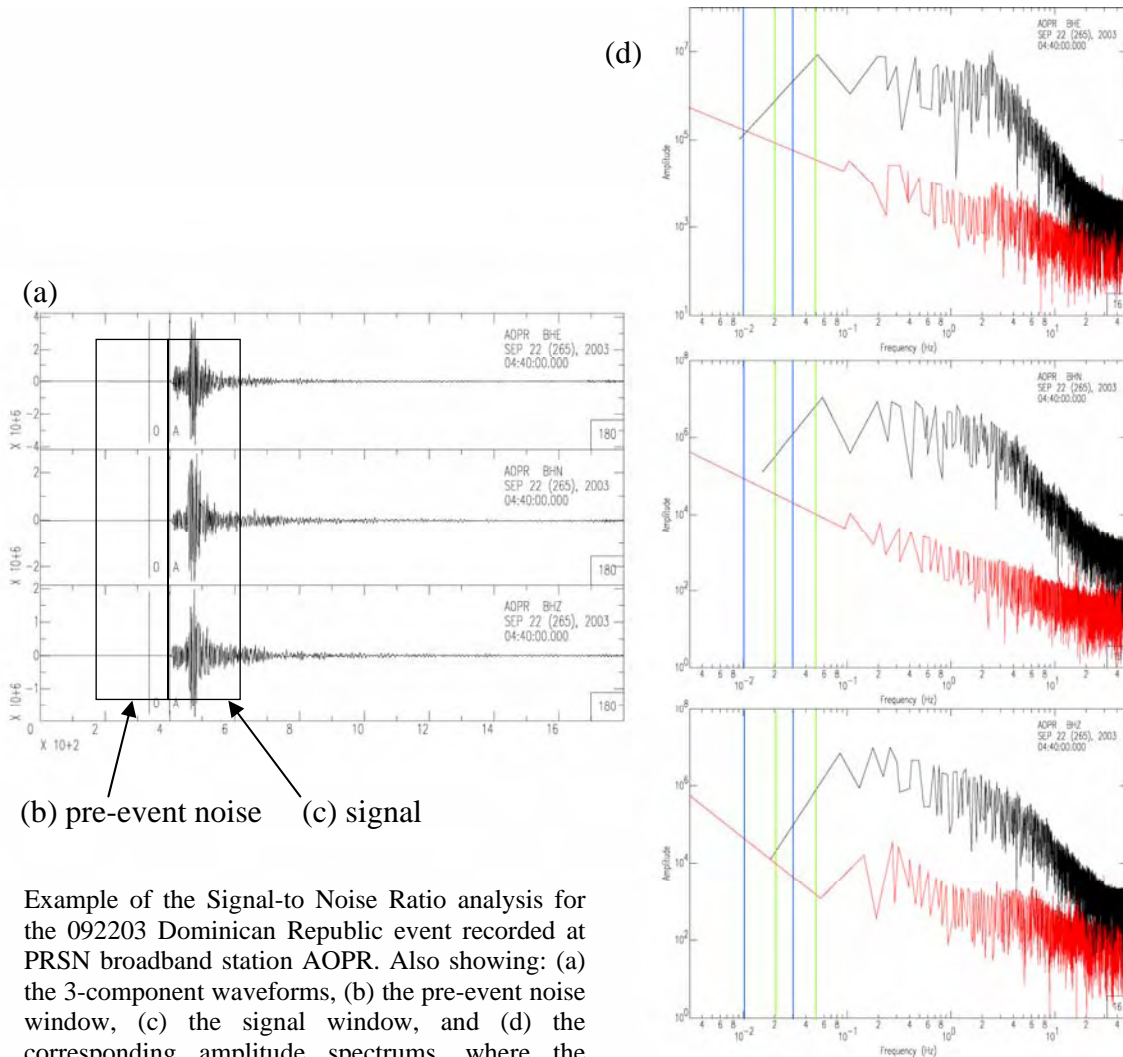
- coastal evolution. Abstract presented at NFS Caribbean Tsunami Workshop, <https://nsfctw.uprm.edu>.
- Nebelek, J., and G. Xia (1995). Moment-tensor analysis using regional data: Application to the 25 March 1993, Scott Mills, Oregon, earthquake, *Geophysical Research Letters* **22**, 13-16.
- Pacheco, J. F., L. R. Sykes (1992). Seismic moment catalog of large earthquakes, 1900 to 1989, *Bull. Seismol, Soc. Am.*, **82**, p.106-1349.
- Puerto Rico Seismic Network (2006). Seismic Catalogue: <http://temblor.uprm.edu/cgi-bin/new-search.cgi>.
- Randall, G. E., Ammon, and Owens, T. J. (1995). Moment tensor estimation using regional seismograms from a Tibetan Plateau portable network development. *Geophys. Res. Lett.*, **22**, p. 1665-1668.
- Reid, H. F., and S. Taber (1919). The Porto Rico earthquakes of October-November, 1918. *Bull. Seism. Soc. Am.*, **9**, p. 95-127.
- Ritsema, J., and T. Lay (1993). Rapid source mechanism determination of large ($M_w \geq 5$) earthquakes in the western United States. *Geophys. Res. Letters*, **20**, 1611-1614.
- Romanowicz, B., D. Dreger, M. Pasyanos, R. Uhrhammer (1993). Monitoring of strain release in central and northern California using broadband data. *Geophys. Res. Letters*, **20**, 1643-1646.
- Schubert, C. (1984). Basin formation along the Boconó-Moron-El Pilar fault system, Venezuela. *Journal of Geophysical Research*, **89**, 5711-5718.
- Smith, W. H. F., and D. T. Sandwell (1997). Global seafloor topography from satellite altimetry and ship depth soundings. *Science*, **277**, 1957-1962.

- ten Brink, U.S. and J. Lin (2004). Stress interaction between subduction earthquakes and forearc strike-slip faults: Modeling and application to the northern Caribbean plate boundary. *J. Geophys. Res.*, **109**, B12310, doi:1029/2004JB003031.
- Thio, H.-K. and H. Kanamori (1995). Moment tensor inversion for local earthquakes using surface waves recorded a terrascop, *Bulletin of the Seismological Society of America*, **85**, 1,021-1,038.
- van der Hirt, Rob., R. Engdahl, W. Sparkman, and G. Nolet (1991). Tomographic imaging of subducted lithosphere below northwest Pacific island arcs, *Nature*, **353**, 37-43
- von Hillebrandt, C. G., and V. Huerfano (2006). Emergent Tsunami warning system for Puerto Rico and the Virgin Islands. In *Caribbean Tsunami Hazards, Proceedings of the NSF Caribbean Tsunami Workshop, San Juan, Puerto Rico, 30-31 March 2004* eds. A. Mercado and P. Liu, 231-243.
- Walter, W. R. (1993). Source parameters of the June 29, 1992 Little Skull Mountain earthquake from complete regional waveforms at a single station, *Geophys. Res. Letters*, **20**, 403-40.

APPENDIX A. EVENTS AND SIGNAL-TO-NOISE RATIO ANALYSIS

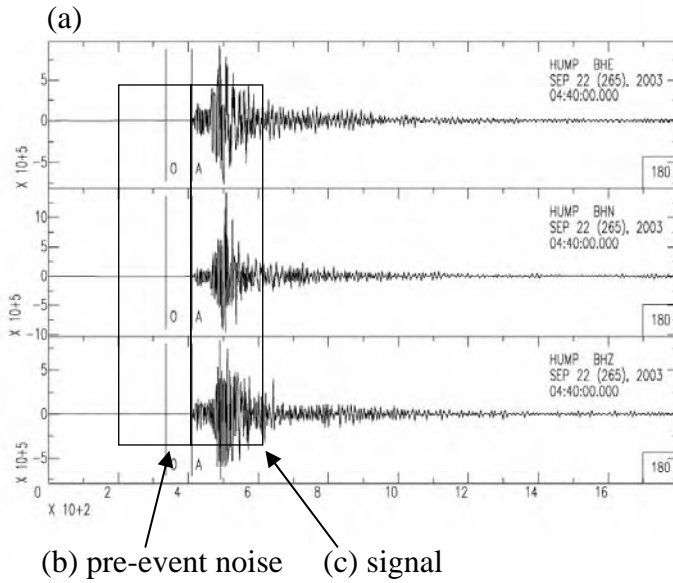
A.1 030922 Dominican Republic Event

A.1.1 Station AOPR

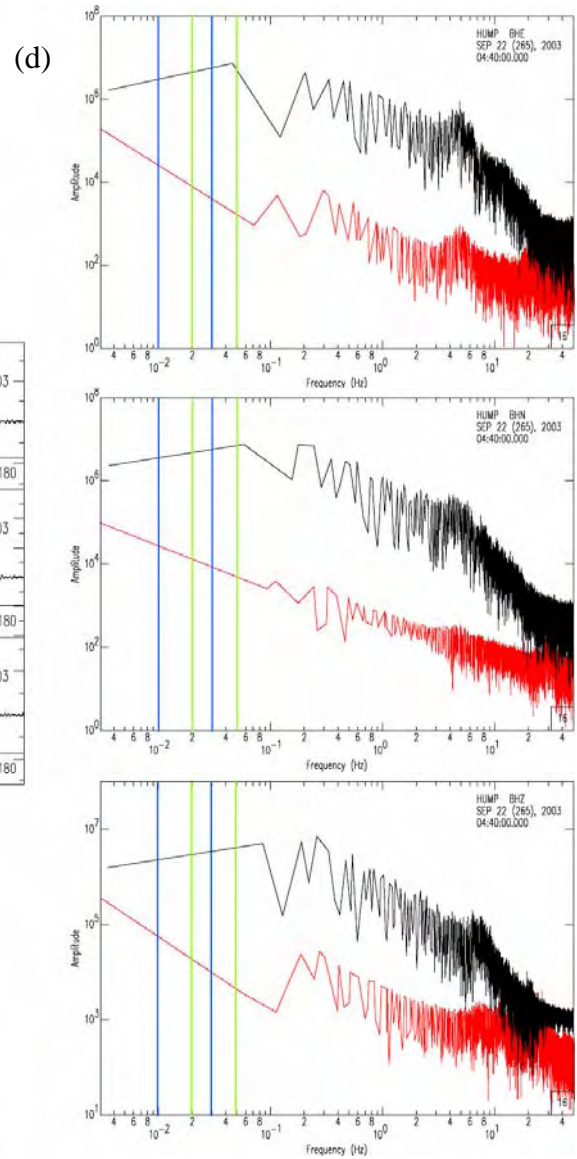


Example of the Signal-to Noise Ratio analysis for the 092203 Dominican Republic event recorded at PRSN broadband station AOPR. Also showing: (a) the 3-component waveforms, (b) the pre-event noise window, (c) the signal window, and (d) the corresponding amplitude spectra, where the signal amplitude spectrum is shown in red, and the pre-event noise amplitude spectrum is shown in black. Bandpass filters are also shown. Blue lines represent 20- to 50- sec bandpass filter, meanwhile green lines represent 30- to 60-sec.

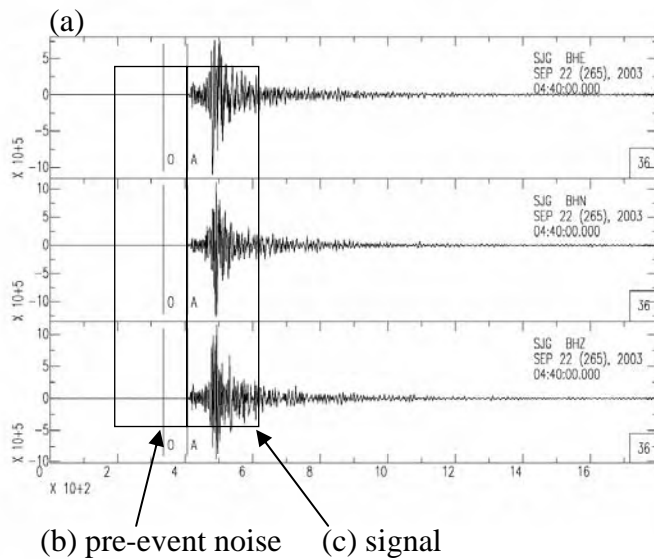
A.1.2 Station HUMP



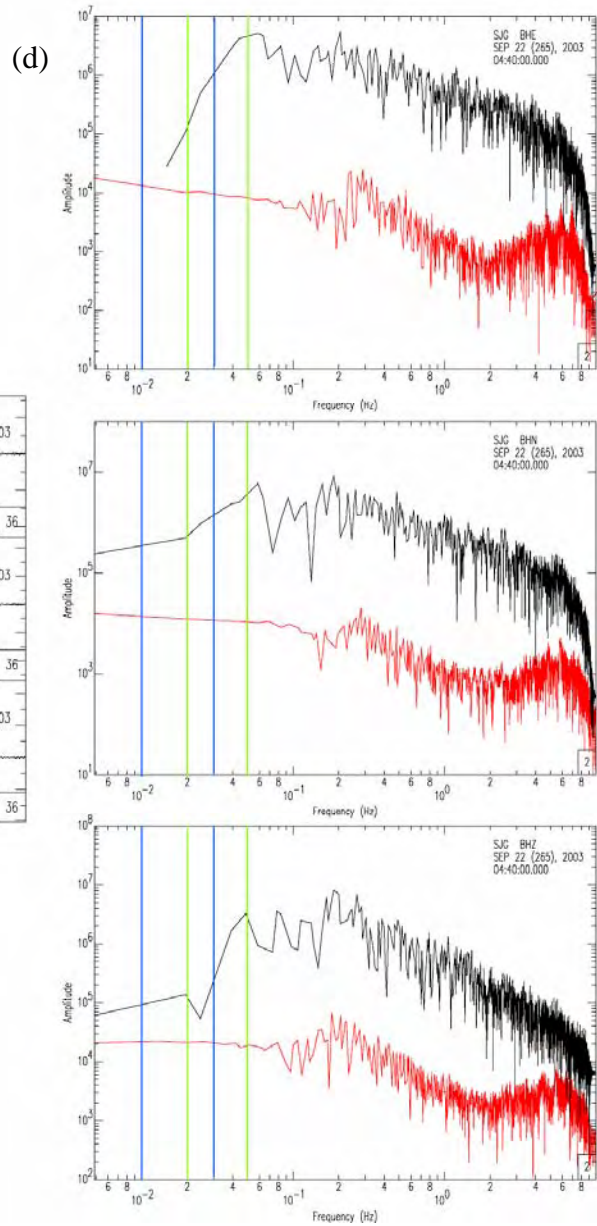
Example of the Signal-to Noise Ratio analysis for the 092203 Dominican Republic event recorded at PRSN broadband station HUMP. Also showing: (a) the 3-component waveforms, (b) the pre-event noise window, (c) the signal window, and (d) the corresponding amplitude spectrums, where the signal amplitude spectrum is shown in red, and the pre-event noise amplitude spectrum is shown in black. Bandpass filters are also shown. Blue lines represent 20- to 50- sec bandpass filter, meanwhile green lines represent 30- to 60-sec.



A.1.3 Station SJG

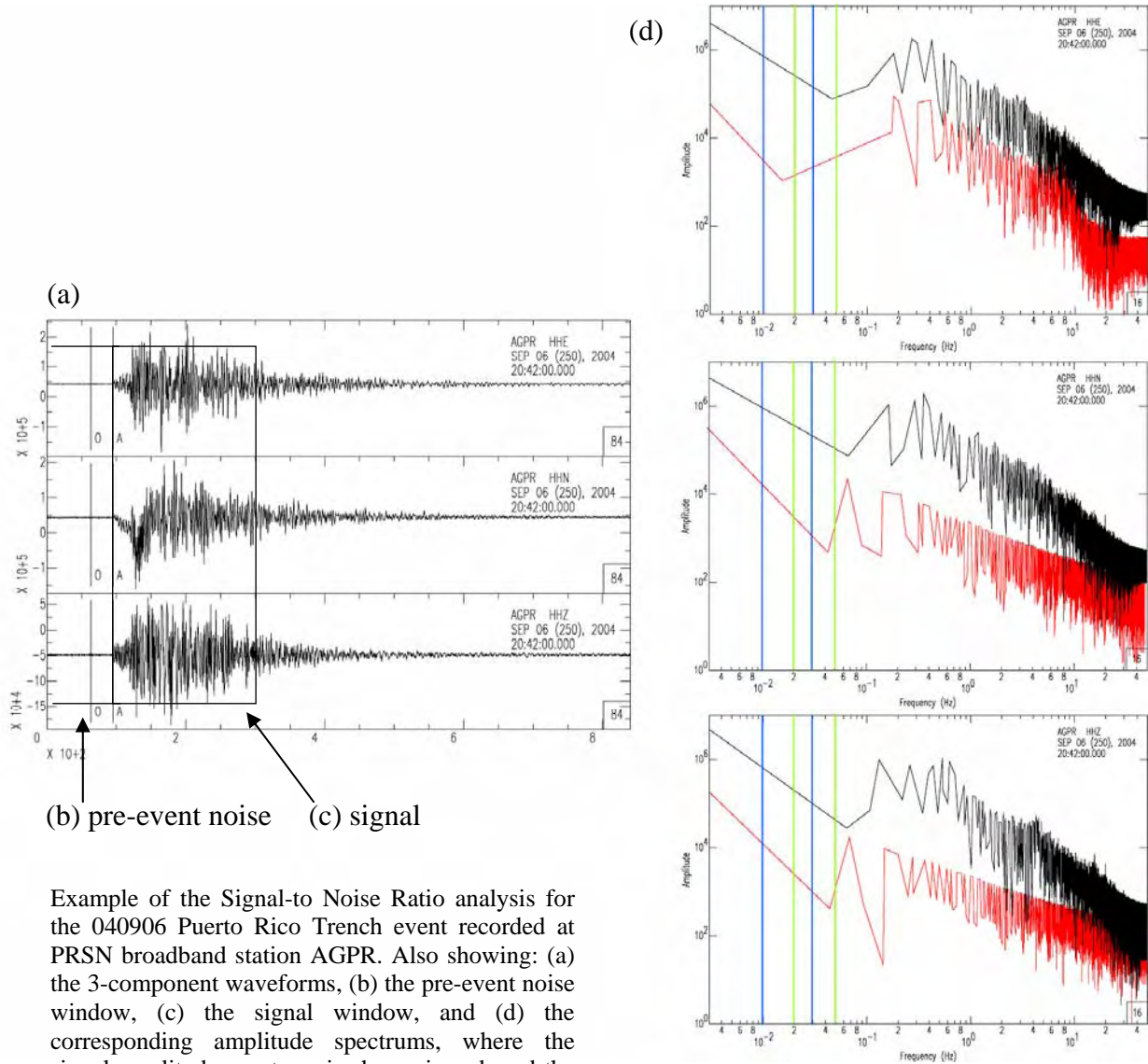


Example of the Signal-to Noise Ratio analysis for the 092203 Dominican Republic event recorded at GSN broadband station SJG. Also showing: (a) the 3-component waveforms, (b) the pre-event noise window, (c) the signal window, and (d) the corresponding amplitude spectrums, where the signal amplitude spectrum is shown in red, and the pre-event noise amplitude spectrum is shown in black. Bandpass filters are also shown. Blue lines represent 20- to 50- sec bandpass filter, meanwhile green lines represent 30- to 60-sec.



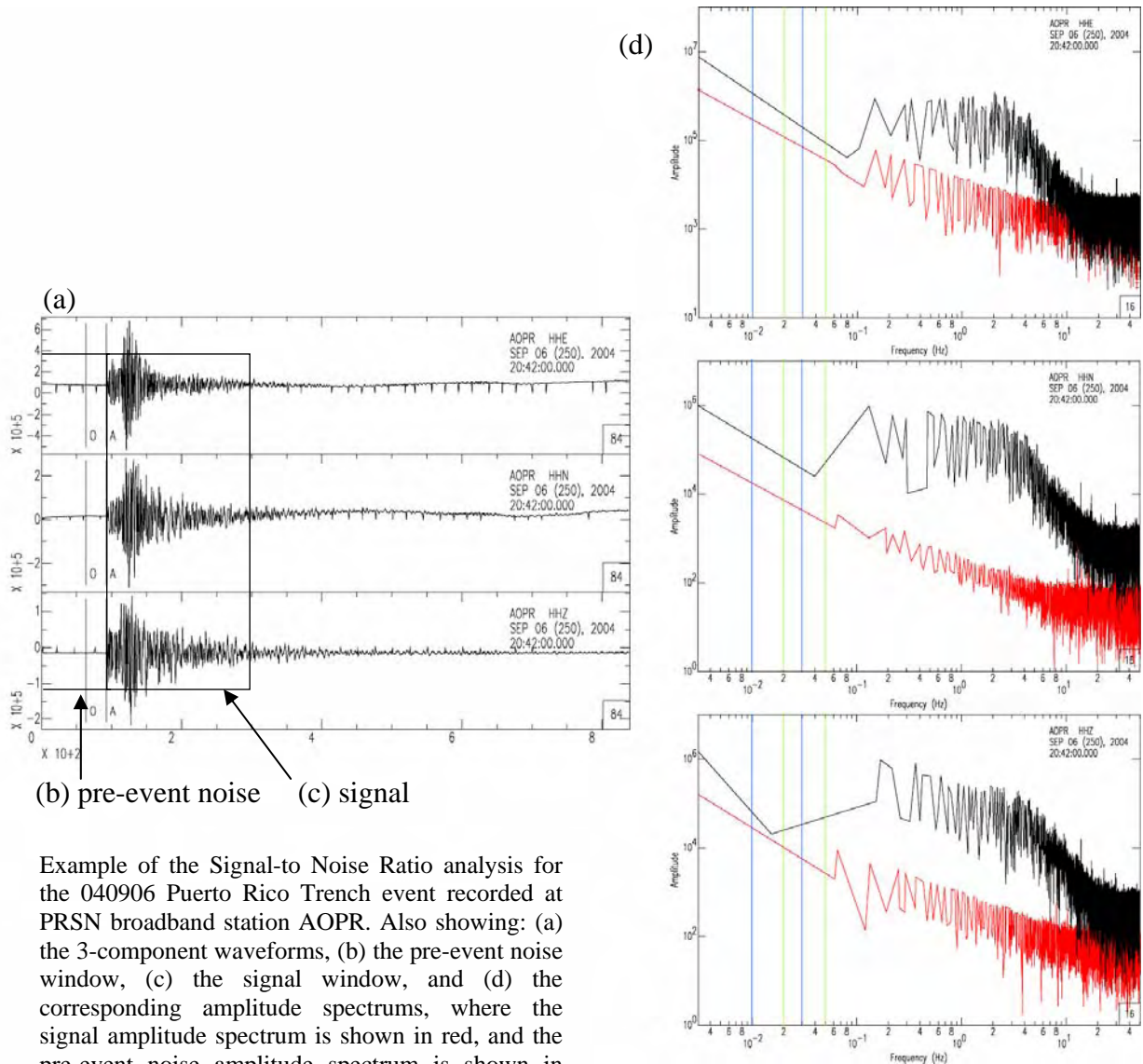
A.2 040906 Puerto Rico Trench Event

A.2.1 Station AGPR



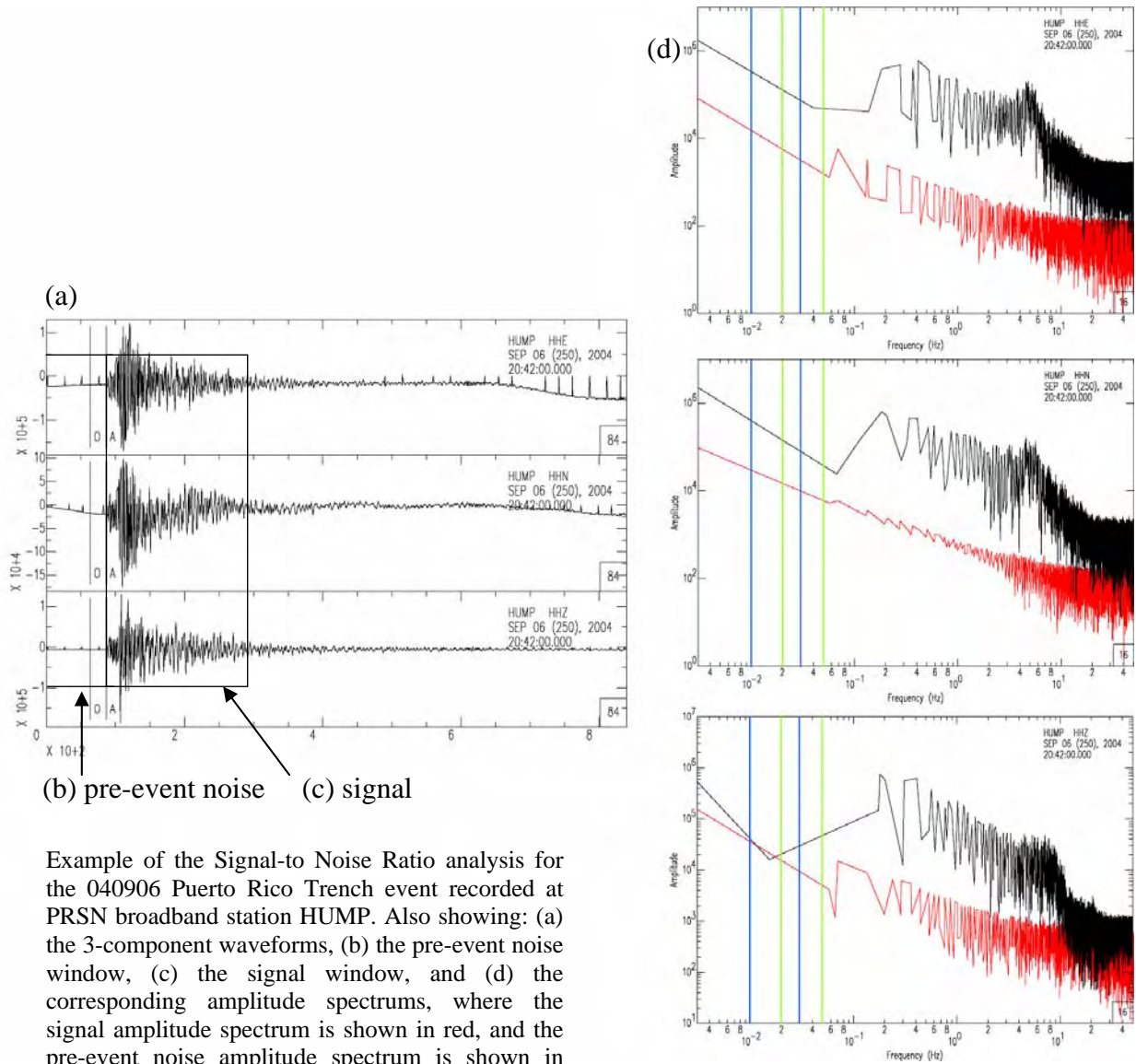
Example of the Signal-to Noise Ratio analysis for the 040906 Puerto Rico Trench event recorded at PRSN broadband station AGPR. Also showing: (a) the 3-component waveforms, (b) the pre-event noise window, (c) the signal window, and (d) the corresponding amplitude spectra, where the signal amplitude spectrum is shown in red, and the pre-event noise amplitude spectrum is shown in black. Bandpass filters are also shown. Blue lines represent 20- to 50- sec bandpass filter, meanwhile green lines represent 30- to 60-sec.

A.2.2 Station AOPR



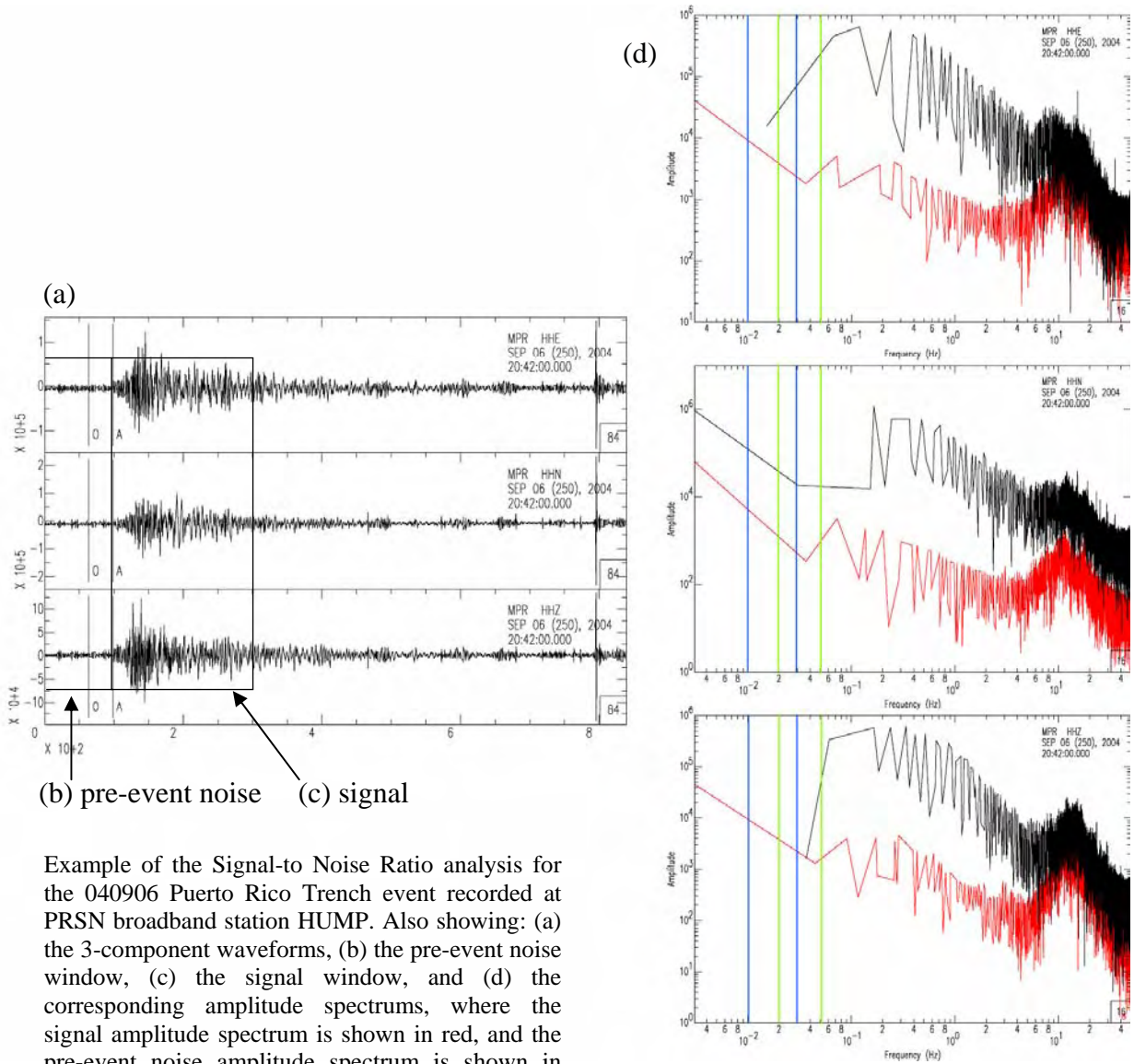
Example of the Signal-to Noise Ratio analysis for the 040906 Puerto Rico Trench event recorded at PRSN broadband station AOPR. Also showing: (a) the 3-component waveforms, (b) the pre-event noise window, (c) the signal window, and (d) the corresponding amplitude spectra, where the signal amplitude spectrum is shown in red, and the pre-event noise amplitude spectrum is shown in black. Bandpass filters are also shown. Blue lines represent 20- to 50- sec bandpass filter, meanwhile green lines represent 30- to 60-sec.

A.2.3 Station HUMP



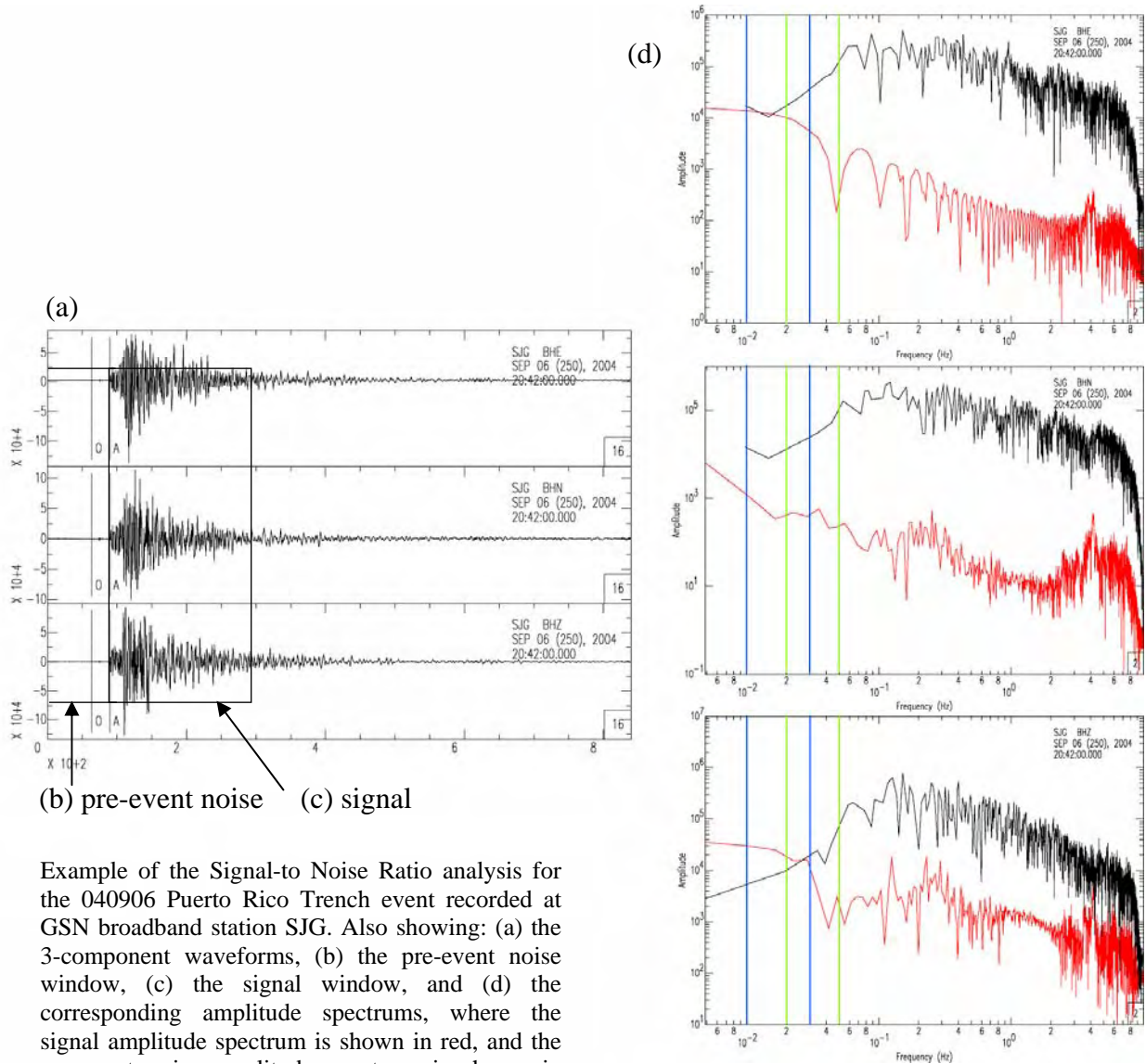
Example of the Signal-to Noise Ratio analysis for the 040906 Puerto Rico Trench event recorded at PRSN broadband station HUMP. Also showing: (a) the 3-component waveforms, (b) the pre-event noise window, (c) the signal window, and (d) the corresponding amplitude spectra, where the signal amplitude spectrum is shown in red, and the pre-event noise amplitude spectrum is shown in black. Bandpass filters are also shown. Blue lines represent 20- to 50- sec bandpass filter, meanwhile green lines represent 30- to 60-sec.

A.2.4 Station MPR



Example of the Signal-to Noise Ratio analysis for the 040906 Puerto Rico Trench event recorded at PRSN broadband station HUMP. Also showing: (a) the 3-component waveforms, (b) the pre-event noise window, (c) the signal window, and (d) the corresponding amplitude spectrums, where the signal amplitude spectrum is shown in red, and the pre-event noise amplitude spectrum is shown in black. Bandpass filters are also shown. Blue lines represent 20- to 50- sec bandpass filter, meanwhile green lines represent 30- to 60-sec.

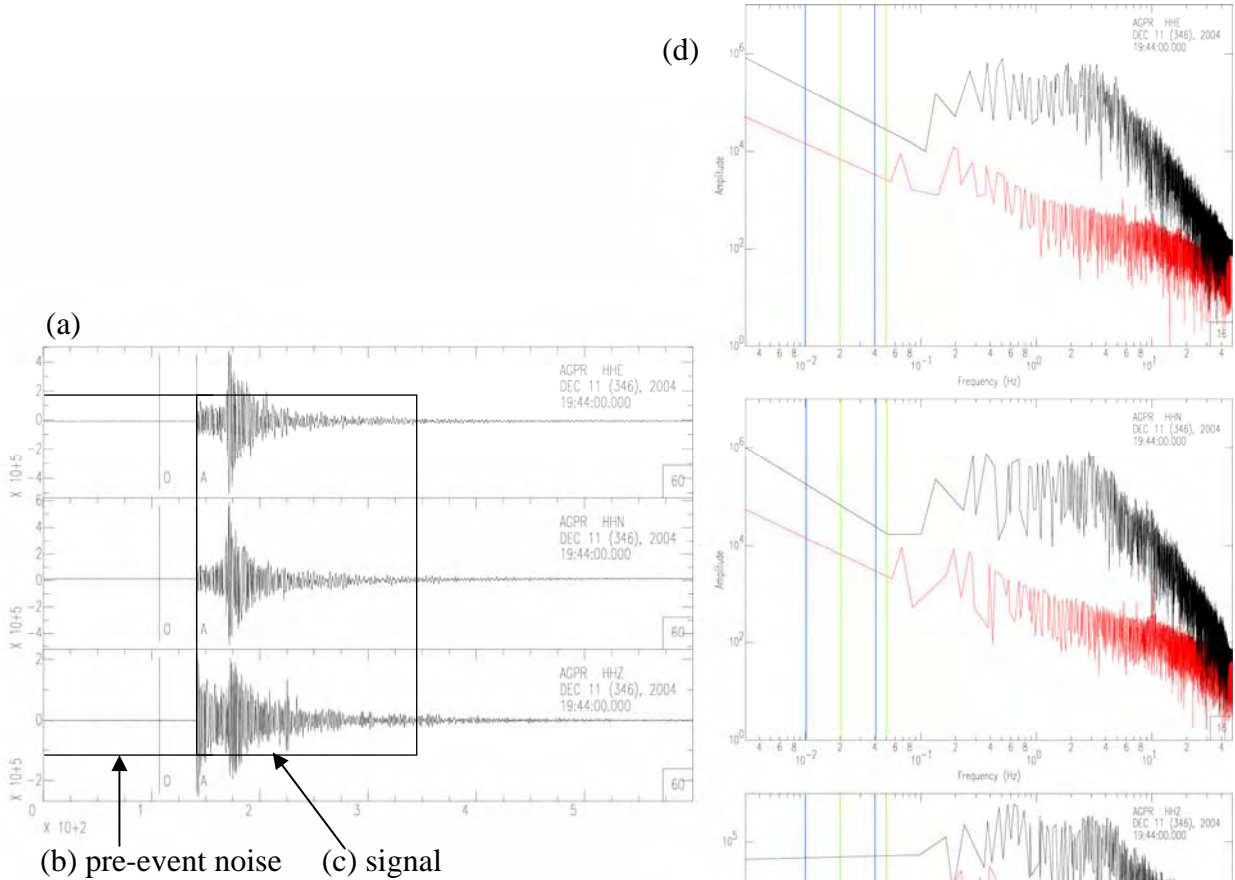
A.2.5 Station SJG



Example of the Signal-to Noise Ratio analysis for the 040906 Puerto Rico Trench event recorded at GSN broadband station SJG. Also showing: (a) the 3-component waveforms, (b) the pre-event noise window, (c) the signal window, and (d) the corresponding amplitude spectrums, where the signal amplitude spectrum is shown in red, and the pre-event noise amplitude spectrum is shown in black. Bandpass filters are also shown. Blue lines represent 20- to 50- sec bandpass filter, meanwhile green lines represent 30- to 60-sec.

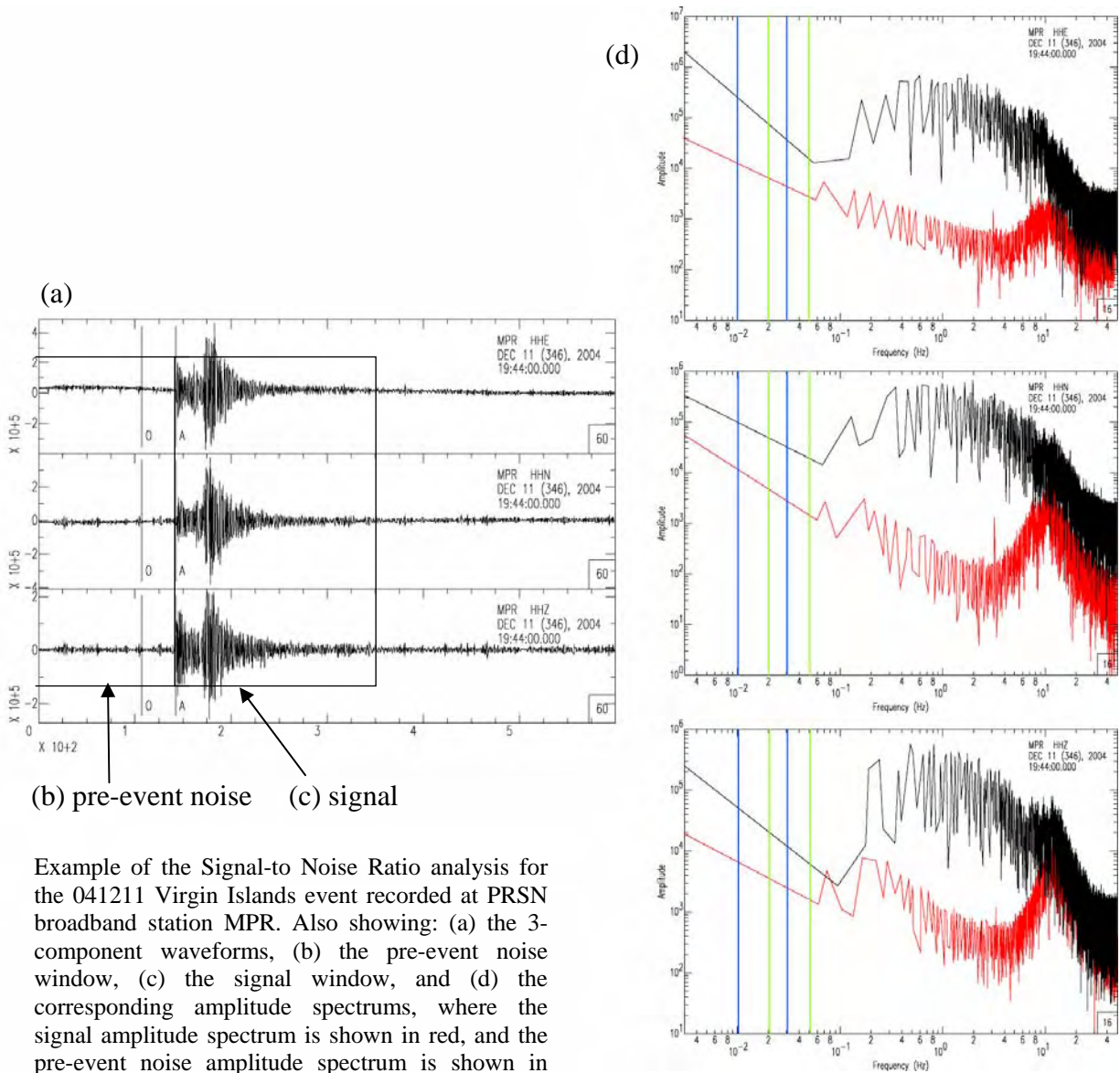
A.3 041211 Virgin Islands Event

A.3.1 Station AGPR



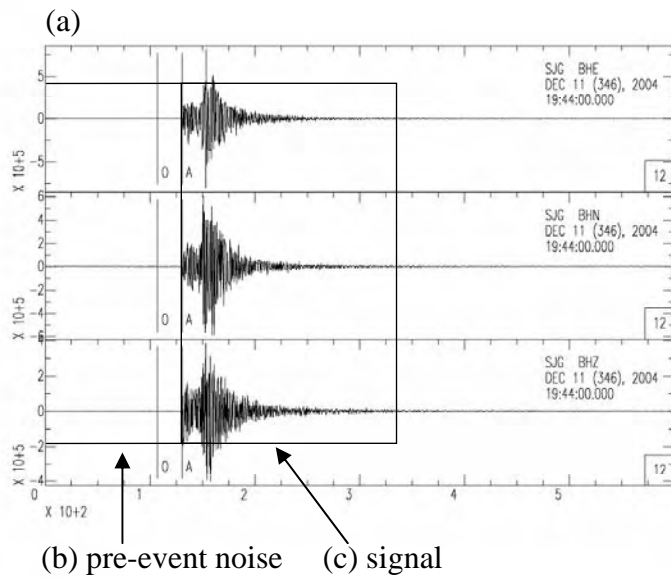
Example of the Signal-to Noise Ratio analysis for the 041211 Virgin Islands event recorded at PRSN broadband station AGPR. Also showing: (a) the 3-component waveforms, (b) the pre-event noise window, (c) the signal window, and (d) the corresponding amplitude spectra, where the signal amplitude spectrum is shown in red, and the pre-event noise amplitude spectrum is shown in black. Bandpass filters are also shown. Blue lines represent 20- to 50- sec bandpass filter, meanwhile green lines represent 30- to 60-sec.

A.3.2 Station MPR

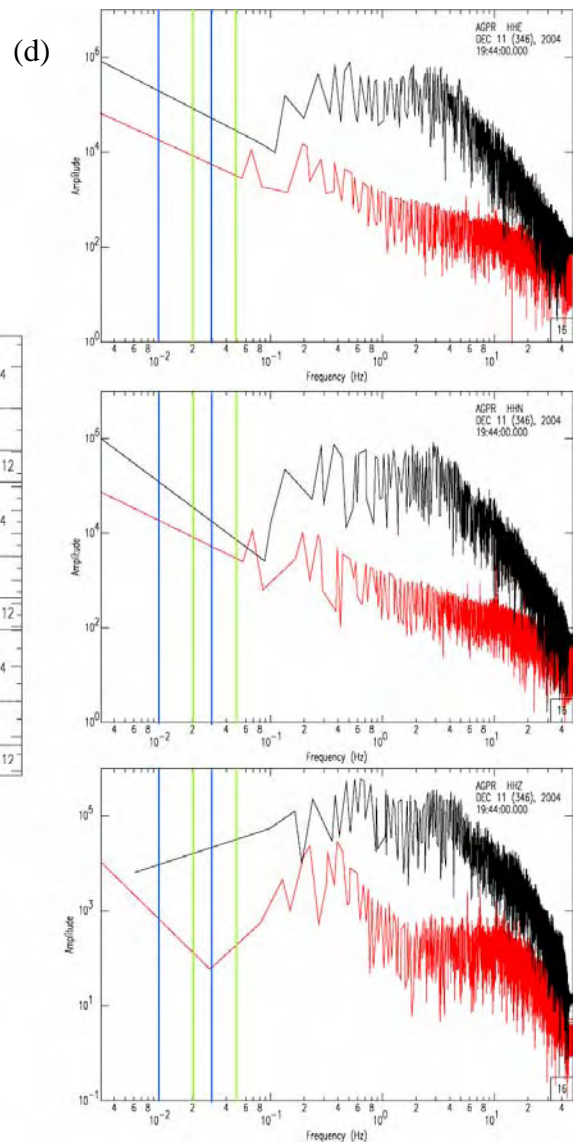


Example of the Signal-to Noise Ratio analysis for the 041211 Virgin Islands event recorded at PRSN broadband station MPR. Also showing: (a) the 3-component waveforms, (b) the pre-event noise window, (c) the signal window, and (d) the corresponding amplitude spectra, where the signal amplitude spectrum is shown in red, and the pre-event noise amplitude spectrum is shown in black. Bandpass filters are also shown. Blue lines represent 20- to 50- sec bandpass filter, meanwhile green lines represent 30- to 60-sec.

A.3.3 Station SJG

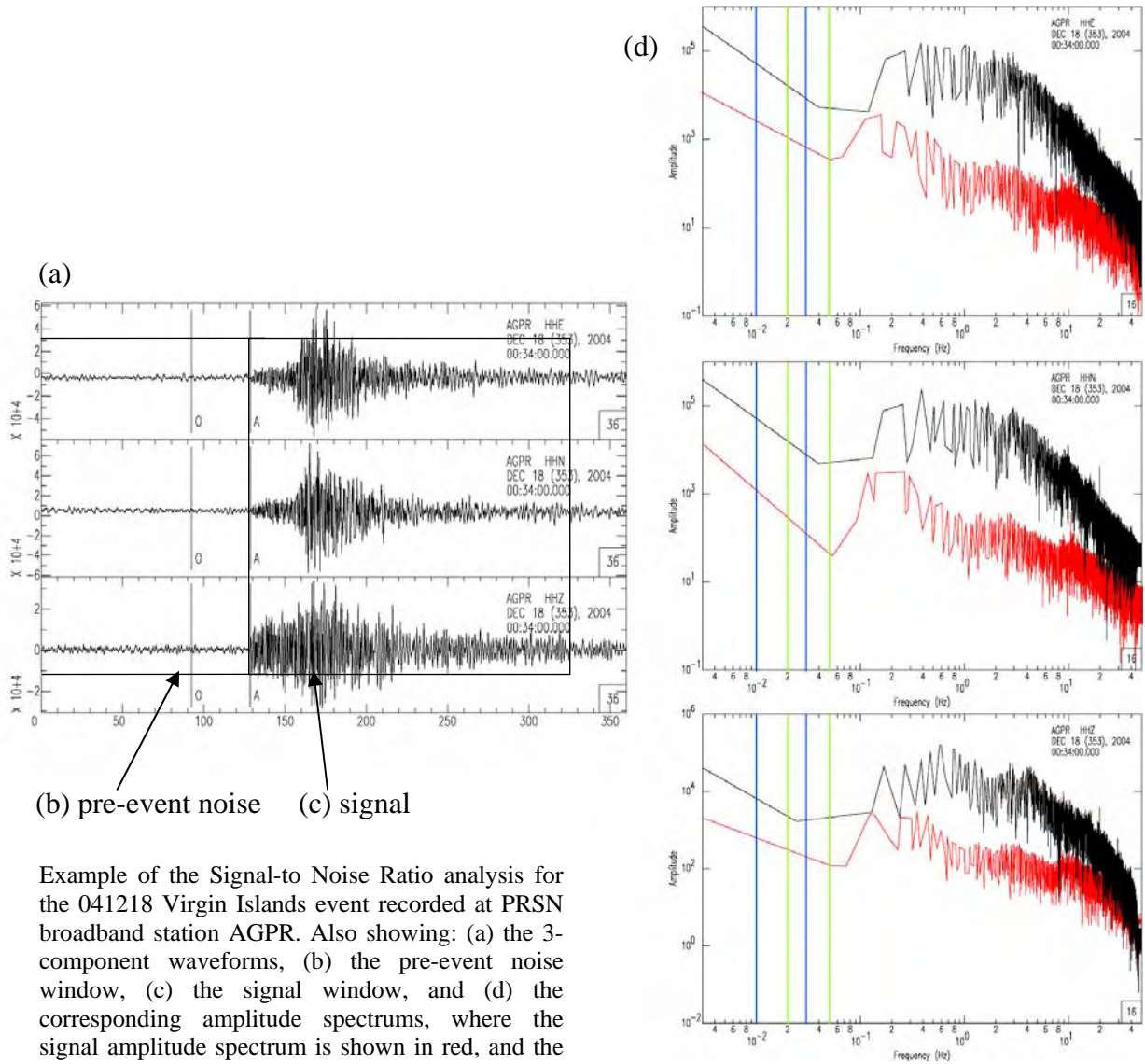


Example of the Signal-to Noise Ratio analysis for the 041211 Virgin Islands event recorded at GSN broadband station SJG. Also showing: (a) the 3-component waveforms, (b) the pre-event noise window, (c) the signal window, and (d) the corresponding amplitude spectrums, where the signal amplitude spectrum is shown in red, and the pre-event noise amplitude spectrum is shown in black. Bandpass filters are also shown. Blue lines represent 20- to 50- sec bandpass filter, meanwhile green lines represent 30- to 60-sec.



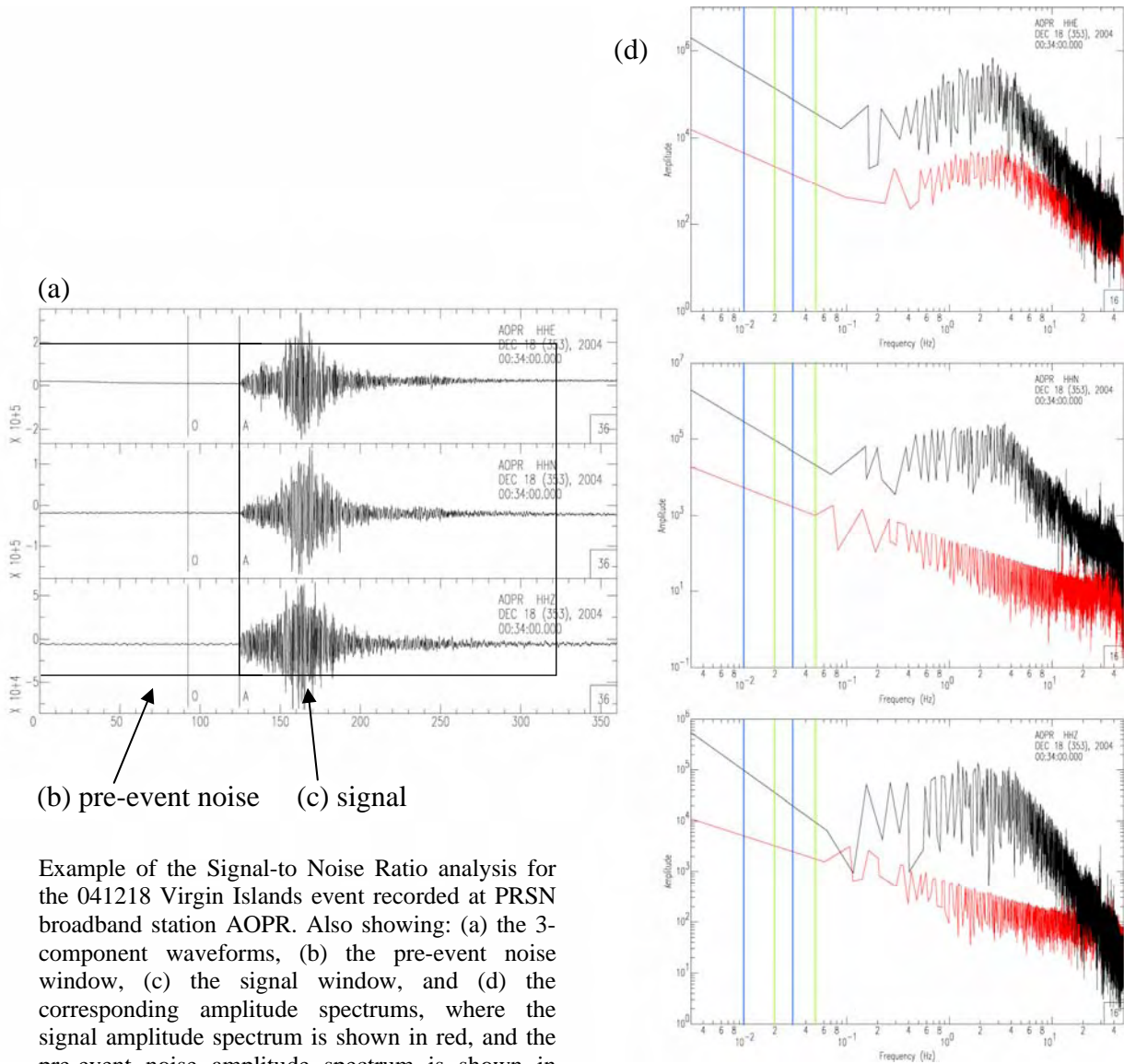
A.4 041218 Virgin Islands Event

A.4.1 Station AGPR



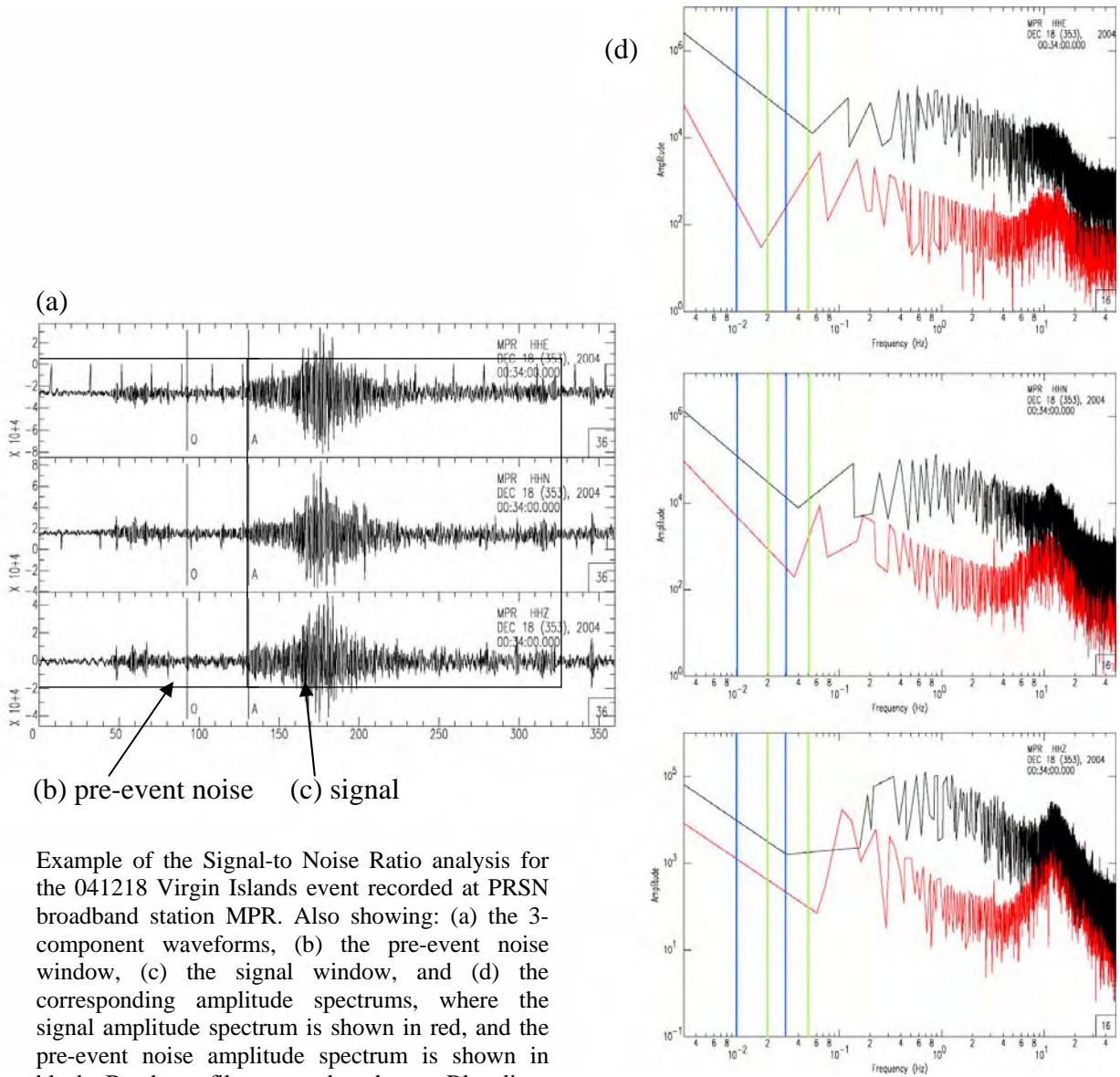
Example of the Signal-to Noise Ratio analysis for the 041218 Virgin Islands event recorded at PRSN broadband station AGPR. Also showing: (a) the 3-component waveforms, (b) the pre-event noise window, (c) the signal window, and (d) the corresponding amplitude spectra, where the signal amplitude spectrum is shown in red, and the pre-event noise amplitude spectrum is shown in black. Bandpass filters are also shown. Blue lines represent 20- to 50- sec bandpass filter, meanwhile green lines represent 30- to 60-sec.

A.4.2 Station AOPR



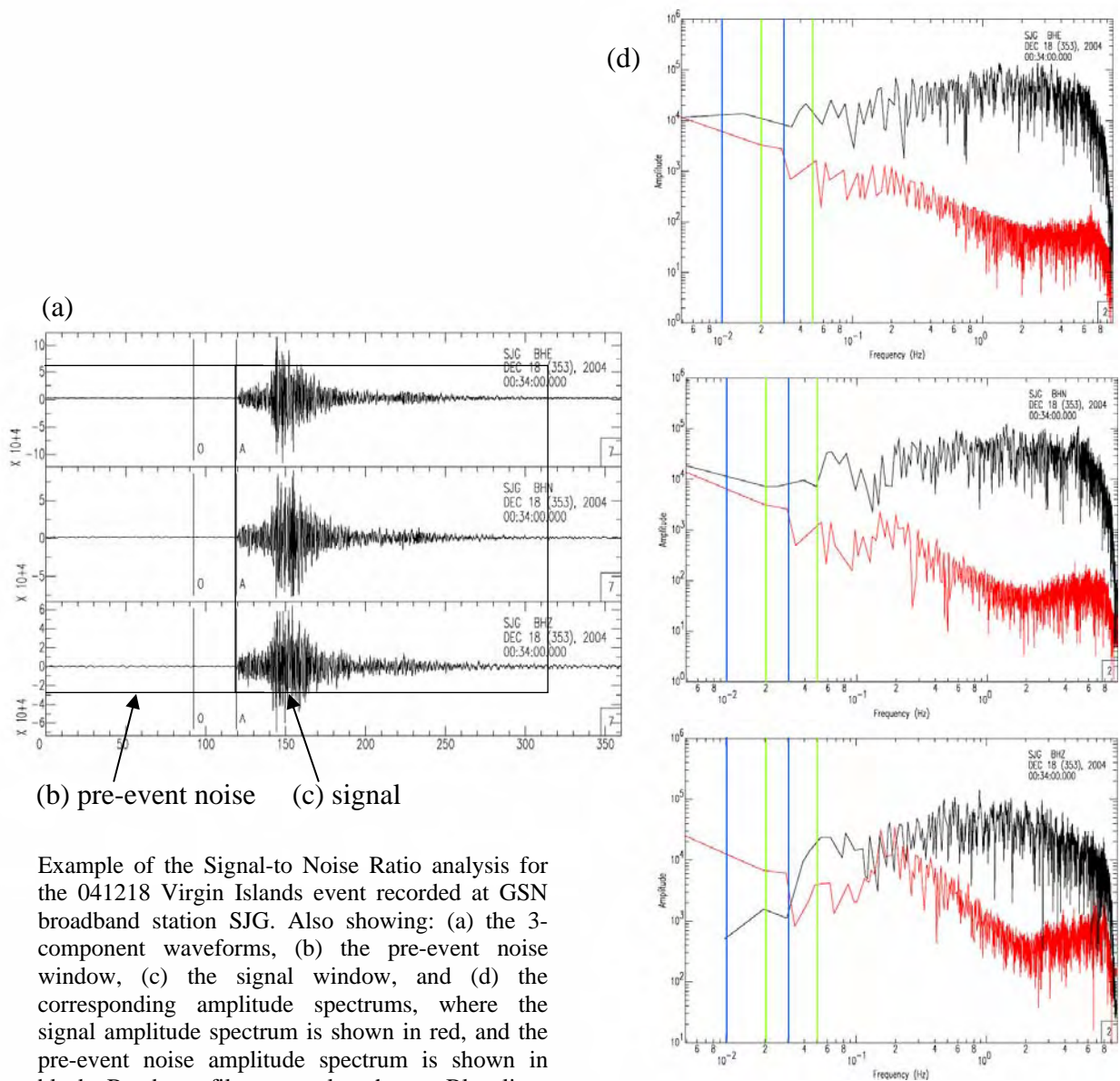
Example of the Signal-to Noise Ratio analysis for the 041218 Virgin Islands event recorded at PRSN broadband station AOPR. Also showing: (a) the 3-component waveforms, (b) the pre-event noise window, (c) the signal window, and (d) the corresponding amplitude spectra, where the signal amplitude spectrum is shown in red, and the pre-event noise amplitude spectrum is shown in black. Bandpass filters are also shown. Blue lines represent 20- to 50- sec bandpass filter, meanwhile green lines represent 30- to 60-sec.

A.4.3 Station MPR



Example of the Signal-to Noise Ratio analysis for the 041218 Virgin Islands event recorded at PRSN broadband station MPR. Also showing: (a) the 3-component waveforms, (b) the pre-event noise window, (c) the signal window, and (d) the corresponding amplitude spectra, where the signal amplitude spectrum is shown in red, and the pre-event noise amplitude spectrum is shown in black. Bandpass filters are also shown. Blue lines represent 20- to 50- sec bandpass filter, meanwhile green lines represent 30- to 60-sec.

A.4.4 Station SJG

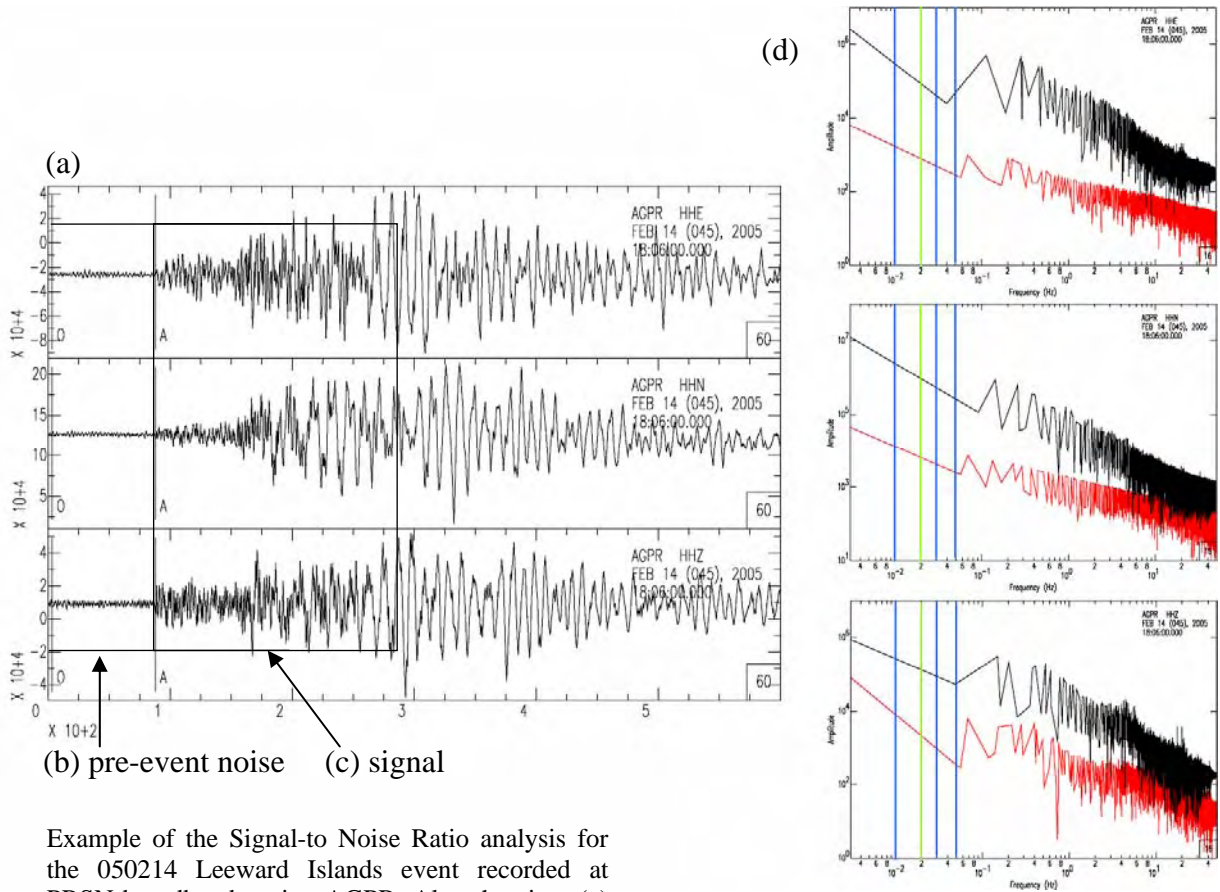


(b) pre-event noise (c) signal

Example of the Signal-to Noise Ratio analysis for the 041218 Virgin Islands event recorded at GSN broadband station SJG. Also showing: (a) the 3-component waveforms, (b) the pre-event noise window, (c) the signal window, and (d) the corresponding amplitude spectrums, where the signal amplitude spectrum is shown in red, and the pre-event noise amplitude spectrum is shown in black. Bandpass filters are also shown. Blue lines represent 20- to 50- sec bandpass filter, meanwhile green lines represent 30- to 60-sec.

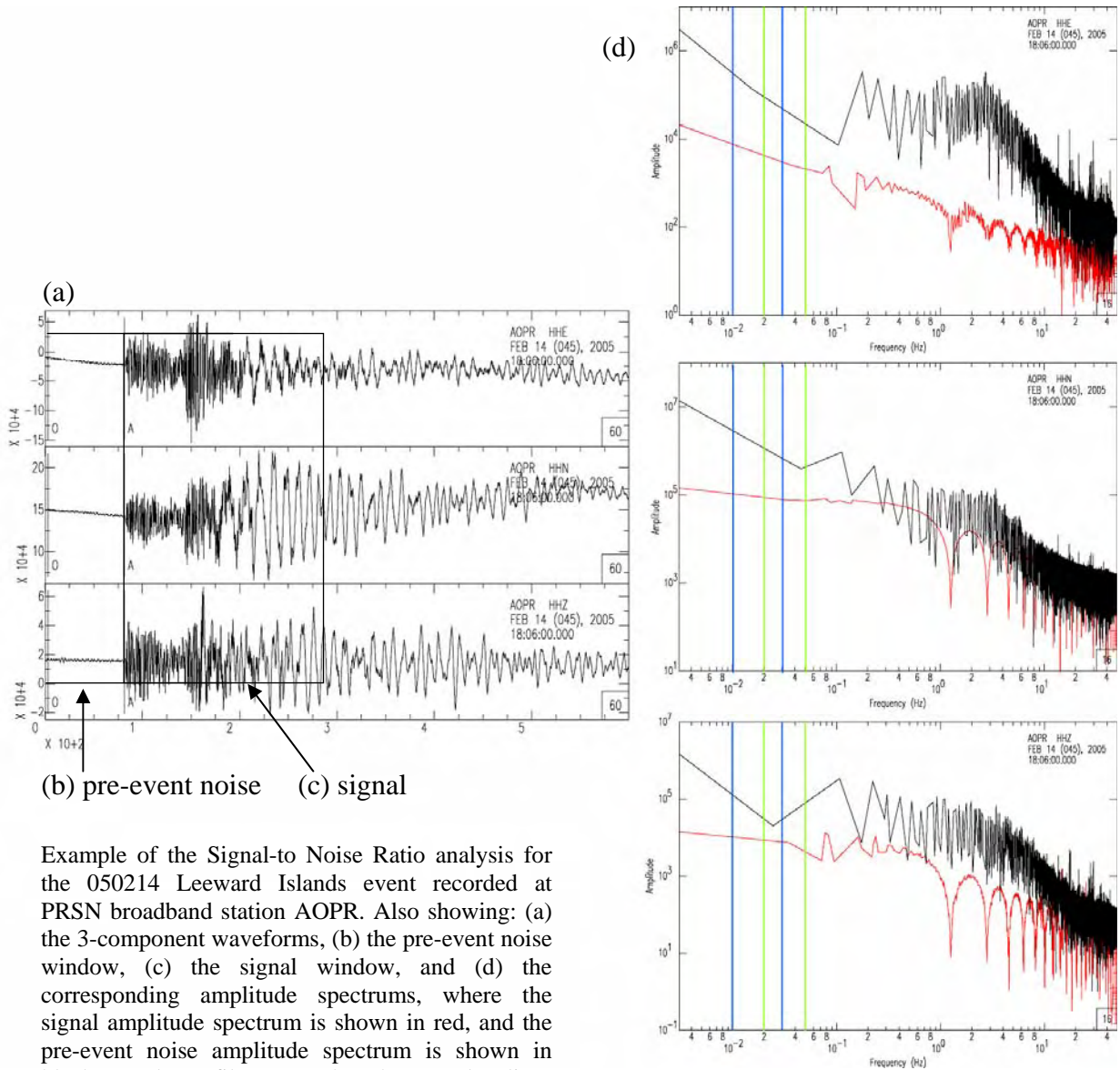
A.5 050214 Leeward Islands Event

A.5.1 Station AGPR



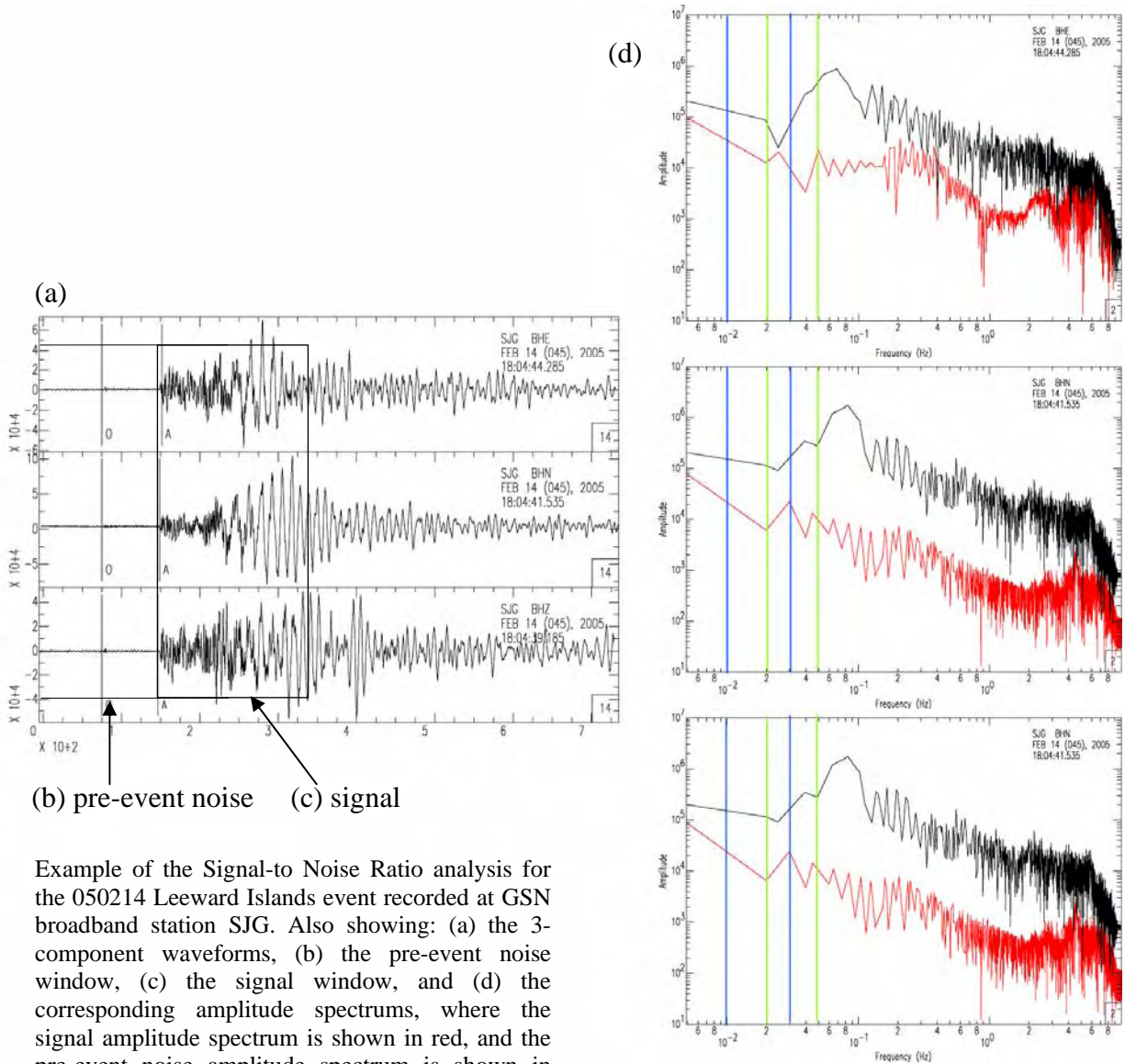
Example of the Signal-to Noise Ratio analysis for the 050214 Leeward Islands event recorded at PRSN broadband station AGPR. Also showing: (a) the 3-component waveforms, (b) the pre-event noise window, (c) the signal window, and (d) the corresponding amplitude spectrums, where the signal amplitude spectrum is shown in red, and the pre-event noise amplitude spectrum is shown in black. Bandpass filters are also shown. Blue lines represent 20- to 50- sec bandpass filter, meanwhile green lines represent 30- to 60-sec.

A.5.2 Station AOPR



Example of the Signal-to Noise Ratio analysis for the 050214 Leeward Islands event recorded at PRSN broadband station AOPR. Also showing: (a) the 3-component waveforms, (b) the pre-event noise window, (c) the signal window, and (d) the corresponding amplitude spectrums, where the signal amplitude spectrum is shown in red, and the pre-event noise amplitude spectrum is shown in black. Bandpass filters are also shown. Blue lines represent 20- to 50- sec bandpass filter, meanwhile green lines represent 30- to 60-sec.

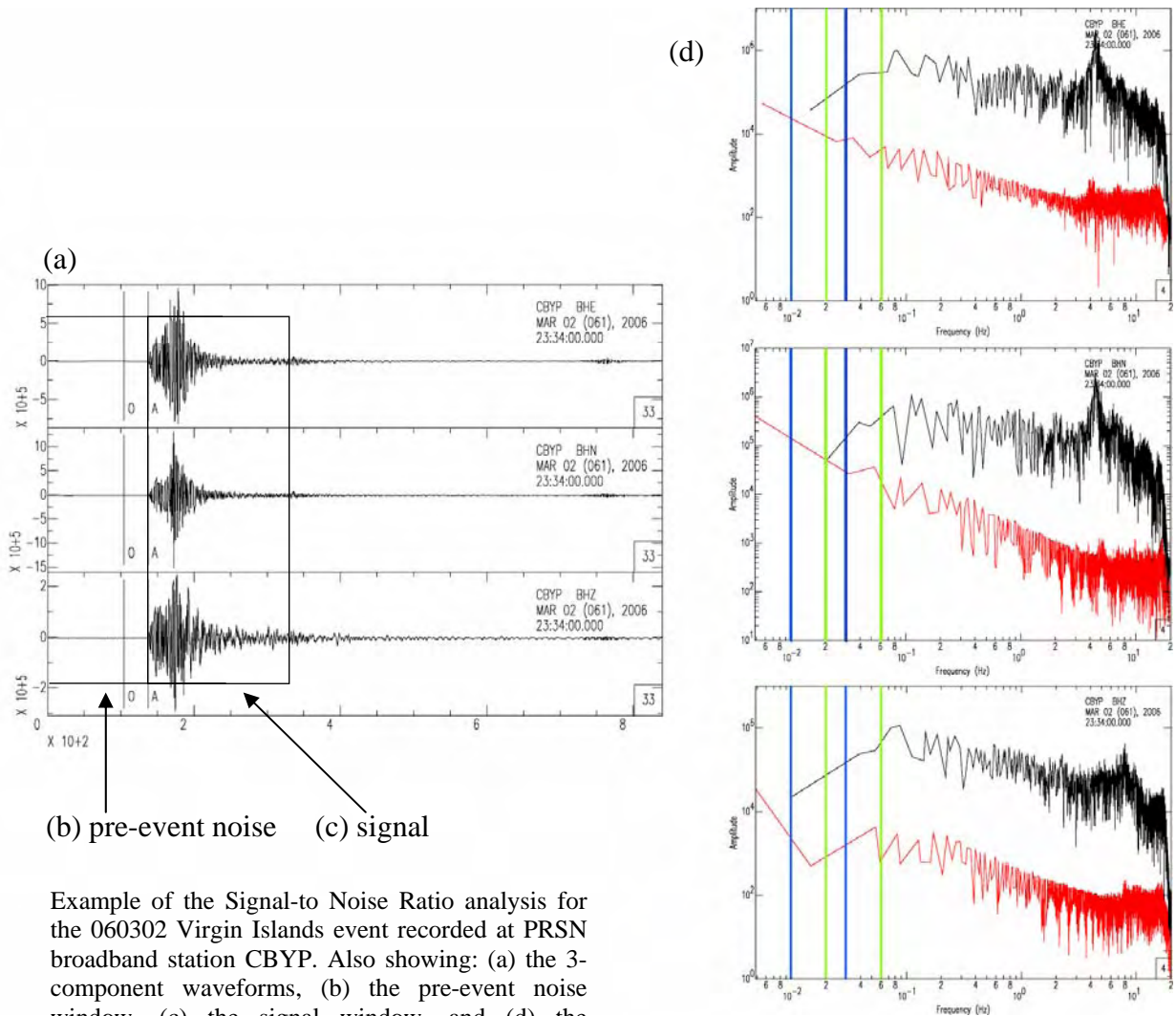
A.5.3 Station SJG



Example of the Signal-to Noise Ratio analysis for the 050214 Leeward Islands event recorded at GSN broadband station SJG. Also showing: (a) the 3-component waveforms, (b) the pre-event noise window, (c) the signal window, and (d) the corresponding amplitude spectra, where the signal amplitude spectrum is shown in red, and the pre-event noise amplitude spectrum is shown in black. Bandpass filters are also shown. Blue lines represent 20- to 50- sec bandpass filter, meanwhile green lines represent 30- to 60-sec.

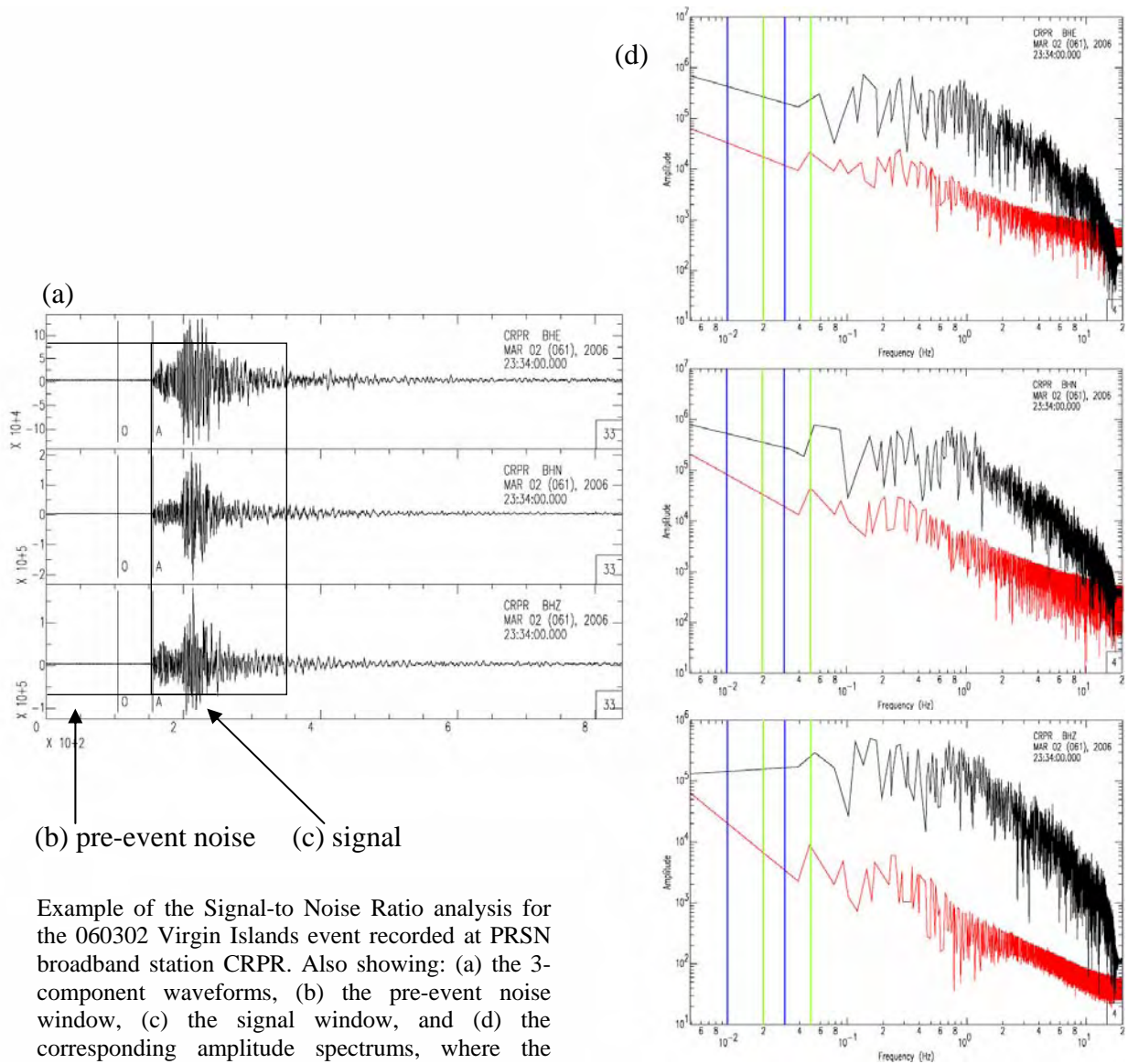
A.6 060302 Virgin Islands Event

A.6.1 Station CBYP



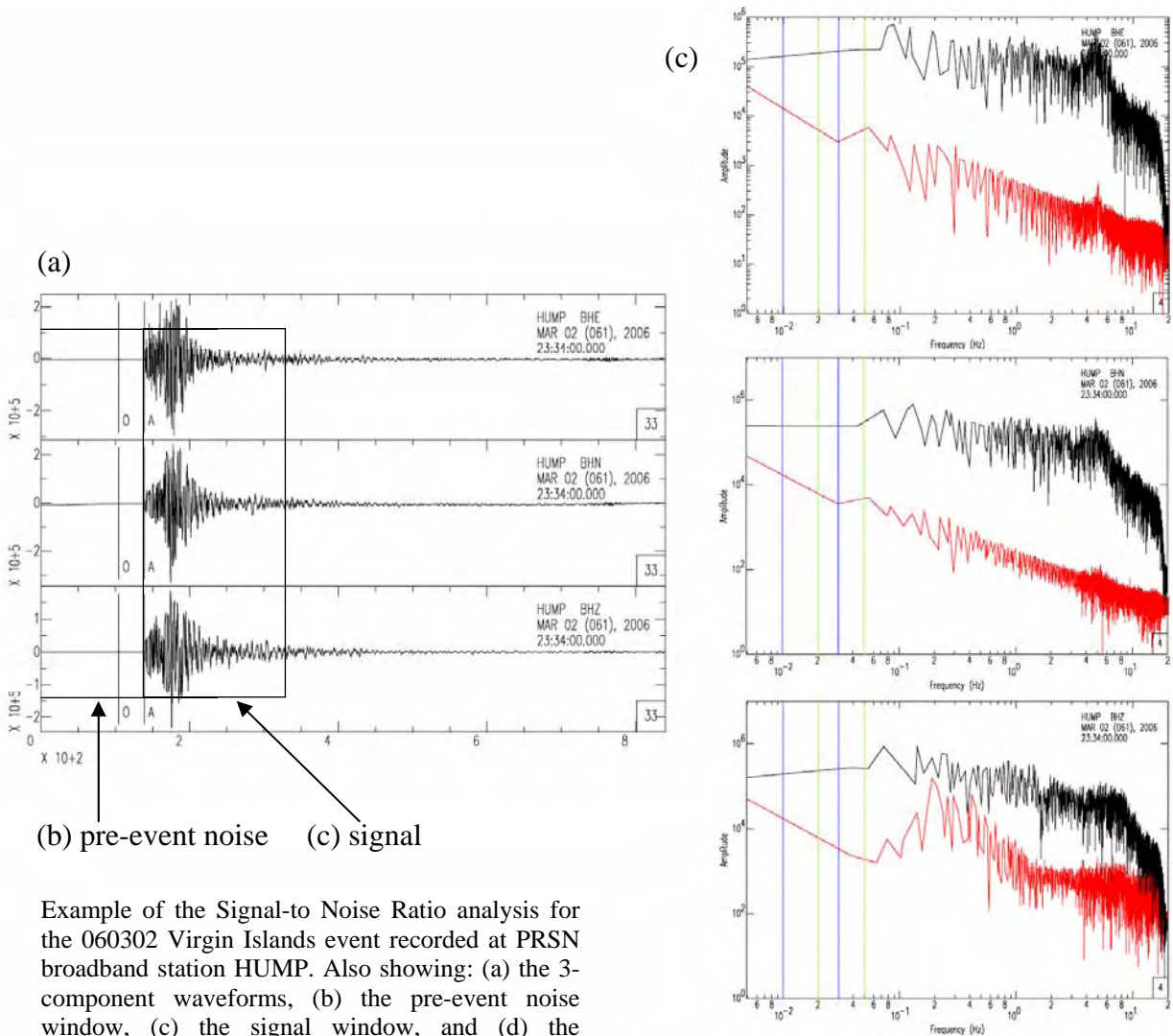
Example of the Signal-to Noise Ratio analysis for the 060302 Virgin Islands event recorded at PRSN broadband station CBYP. Also showing: (a) the 3-component waveforms, (b) the pre-event noise window, (c) the signal window, and (d) the corresponding amplitude spectra, where the signal amplitude spectrum is shown in red, and the pre-event noise amplitude spectrum is shown in black. Bandpass filters are also shown. Blue lines represent 20- to 50- sec bandpass filter, meanwhile green lines represent 30- to 60-sec.

A.6.2 Station CRPR



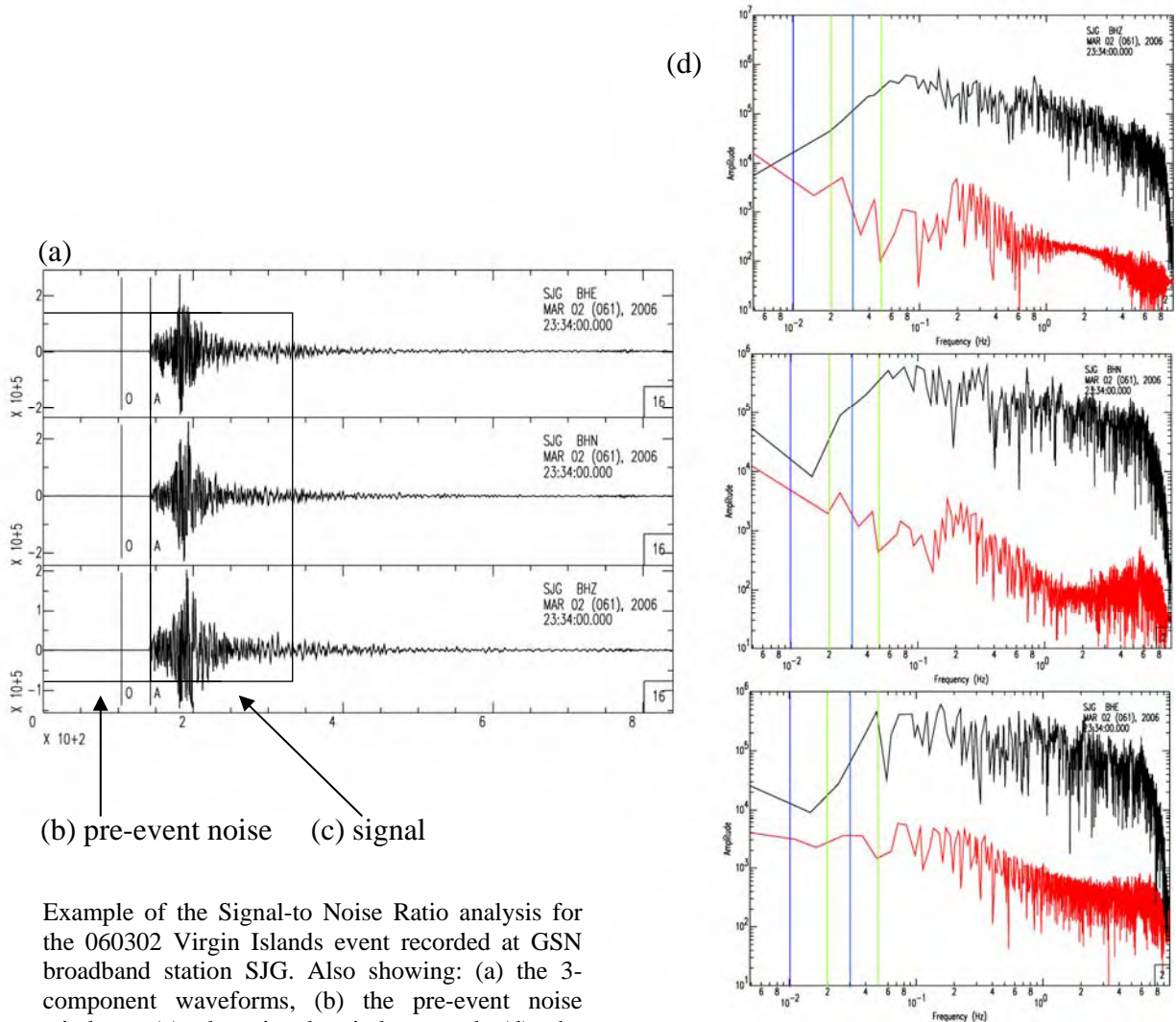
Example of the Signal-to Noise Ratio analysis for the 060302 Virgin Islands event recorded at PRSN broadband station CRPR. Also showing: (a) the 3-component waveforms, (b) the pre-event noise window, (c) the signal window, and (d) the corresponding amplitude spectra, where the signal amplitude spectrum is shown in red, and the pre-event noise amplitude spectrum is shown in black. Bandpass filters are also shown. Blue lines represent 20- to 50- sec bandpass filter, meanwhile green lines represent 30- to 60-sec.

A.6.3 Station HUMP



Example of the Signal-to Noise Ratio analysis for the 060302 Virgin Islands event recorded at PRSN broadband station HUMP. Also showing: (a) the 3-component waveforms, (b) the pre-event noise window, (c) the signal window, and (d) the corresponding amplitude spectrums, where the signal amplitude spectrum is shown in red, and the pre-event noise amplitude spectrum is shown in black. Bandpass filters are also shown. Blue lines represent 20- to 50- sec bandpass filter, meanwhile green lines represent 30- to 60-sec.

A.6.4 Station SJG



Example of the Signal-to Noise Ratio analysis for the 060302 Virgin Islands event recorded at GSN broadband station SJG. Also showing: (a) the 3-component waveforms, (b) the pre-event noise window, (c) the signal window, and (d) the corresponding amplitude spectra, where the signal amplitude spectrum is shown in red, and the pre-event noise amplitude spectrum is shown in black. Bandpass filters are also shown. Blue lines represent 20- to 50- sec bandpass filter, meanwhile green lines represent 30- to 60-sec.

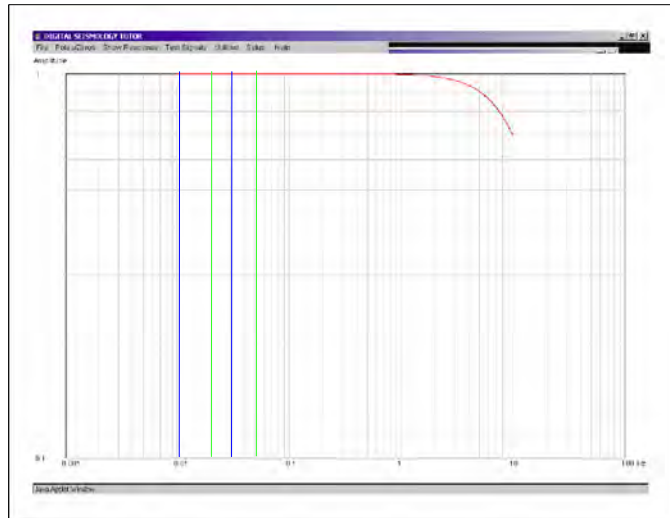
APPENDIX B INSTRUMENT RESPONSES

B.1 Instrument response for the PRSN broadband station CBYP. The station was normalized to 1. Blue and green lines represent the frequency bandpass utilized in the RMT inversion.

Station CBYP			
BHE Channel			
Poles		Zeros	
Real	Imaginary	Real	Imaginary
-5.02655E+02	0	0	0
-1.01531E+03	0	0	0
-1.13097E+03	0		
-4.44221E-02	4.44221E-02		
-4.44221E-02	-4.44221E-02		
Constant			
5.95183E+17			

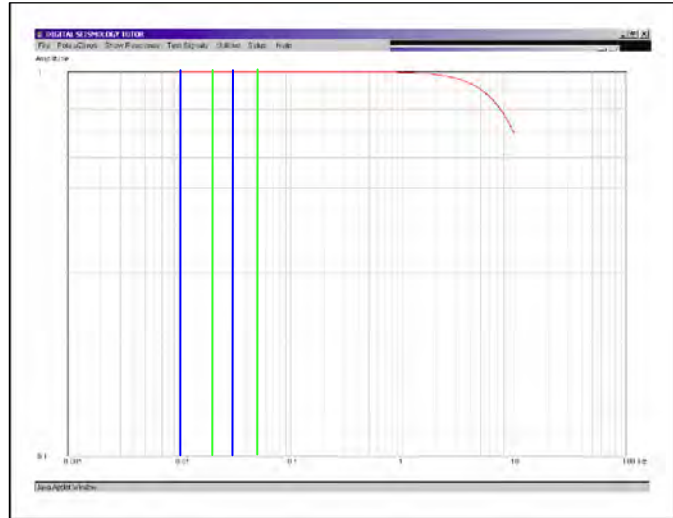
Station CBYP			
BHN Channel			
Poles		Zeros	
Real	Imaginary	Real	Imaginary
-5.02655E+02	0	0	0
-1.00531E+03	0	0	0
-1.13097E+03	0		
-4.44221E-02	4.44221E-02		
-4.44221E-02	-4.44221E-02		
Constant			
5.59582E+17			

Station CBYP			
BHZ Channel			
Poles		Zeros	
Real	Imaginary	Real	Imaginary
-5.02655E+02	0	0	0
-1.00531E+03	0	0	0
-1.13097E+03	0		
-4.44221E-02	4.44221E-02		
-4.44221E-02	-4.44221E-02		
Constant			
5.94584E+17			



B.2 Instrument response for the PRSN broadband station CRPR. The station was normalized to 1. Blue and green lines represent the frequency bandpass utilized in the RMT inversion.

Station CRPR BHE Channel				
Poles		Zeros		
Real	Imaginary	Real	Imaginary	
-5.02655E+02	0	0	0	
-1.01531E+03	0	0	0	
-1.13097E+03	0			
-4.44221E-02	4.44221E-02			
-4.44221E-02	-4.44221E-02			
Constant				
5.60830E+17				
Station CRPR BHN Channel				
Poles		Zeros		
Real	Imaginary	Real	Imaginary	
-5.02655E+02	0	0	0	
-1.00531E+03	0	0	0	
-1.13097E+03	0			
-4.44221E-02	4.44221E-02			
-4.44221E-02	-4.44221E-02			
Constant				
5.591450E+17				
Station CRPR BHZ Channel				
Poles		Zeros		
Real	Imaginary	Real	Imaginary	
-5.02655E+02	0	0	0	
-1.00531E+03	0	0	0	
-1.13097E+03	0			
-4.44221E-02	4.44221E-02			
-4.44221E-02	-4.44221E-02			
Constant				
5.56897E+17				

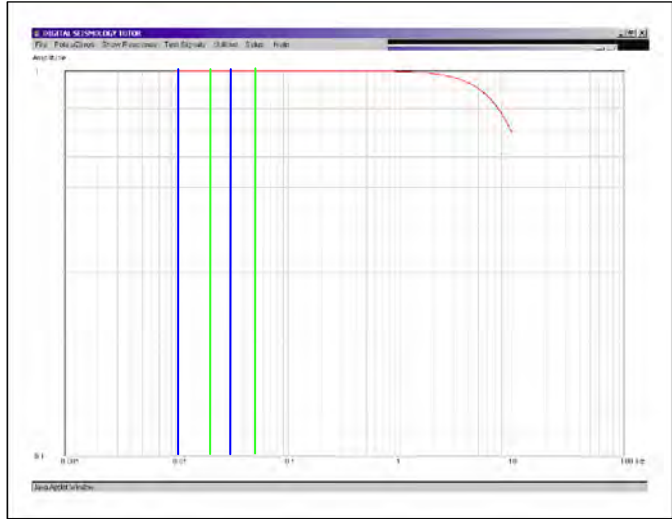


B.3 Instrument response for the PRSN broadband station AOPR. The station was normalized to 1. Blue and Green lines represent the frequency bandpass utilized in the RMT inversion.

Station AOPR			
BHE Channel			
Poles		Zeros	
Real	Imaginary	Real	Imaginary
-5.02655E+02	0	0	0
-1.00531E+03	0	0	0
-1.13097E+03	0		
-1.23402E-02	1.23402E-02		
-1.23402E-02	-1.23402E-02		
Constant			
5.30543E+17			

Station AOPR			
BHN Channel			
Poles		Zeros	
Real	Imaginary	Real	Imaginary
-5.02655E+02	0	0	0
-1.00531E+03	0	0	0
-1.13097E+03	0		
-1.23402E-02	1.23402E-02		
-1.23402E-02	-1.23402E-02		
Constant			
7.16250E+17			

Station AOPR			
BHZ Channel			
Poles		Zeros	
Real	Imaginary	Real	Imaginary
-5.02655E+02	0	0	0
-1.00531E+03	0	0	0
-1.13097E+03	0		
-1.23402E-02	1.23402E-02		
-1.23402E-02	-1.23402E-02		
Constant			
5.29105E+17			

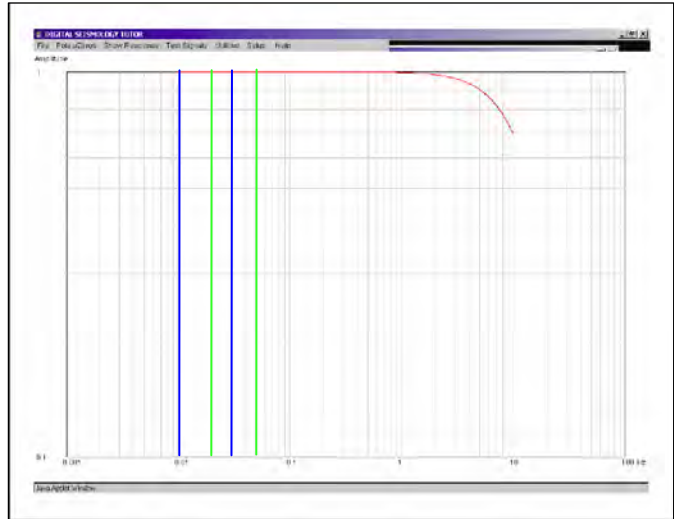


B.4 Instrument response for the PRSN broadband station AGPR. The station was normalized to 1. Blue and Green lines represent the frequency bandpass utilized in the RMT inversion.

Station AGPR BHE Channel			
Poles		Zeros	
Real	Imaginary	Real	Imaginary
-5.02655E+02	0	0	0
-1.00531E+03	0	0	0
-1.13097E+03	0		
-1.23402E-02	1.23402E-02		
-1.23402E-02	-1.23402E-02		
Constant			
5.29824E+17			

Station AGPR BHN Channel			
Poles		Zeros	
Real	Imaginary	Real	Imaginary
-5.02655E+02	0	0	0
-1.00531E+03	0	0	0
-1.13097E+03	0		
-1.23402E-02	1.23402E-02		
-1.23402E-02	-1.23402E-02		
Constant			
5.20478E+17			

Station AGPR BHZ Channel			
Poles		Zeros	
Real	Imaginary	Real	Imaginary
-5.02655E+02	0	0	0
-1.00531E+03	0	0	0
-1.13097E+03	0		
-1.23402E-02	1.23402E-02		
-1.23402E-02	-1.23402E-02		
Constant			
5.28386E+17			

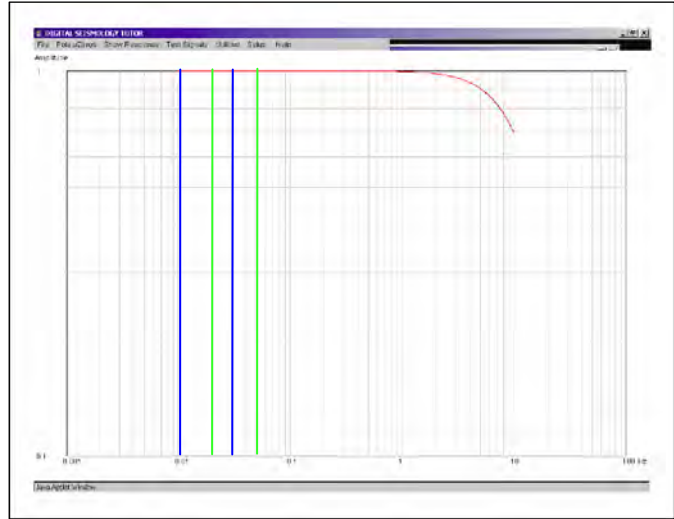


B.5 Instrument response for the PRSN broadband station HUMP. The station was normalized to 1. Blue and Green lines represent the frequency bandpass utilized in the RMT inversion.

Station HUMP				
BHE Channel				
Poles		Zeros		
Real	Imaginary	Real	Imaginary	
-5.02655E+02	0	0	0	
-1.00531E+03	0	0	0	
-1.13097E+03	0			
-1.23402E-02	1.23402E-02			
-1.23402E-02	-1.23402E-02			
Constant				
5.262230E+17				

Station HUMP				
BHN Channel				
Poles		Zeros		
Real	Imaginary	Real	Imaginary	
-5.02655E+02	0	0	0	
-1.00531E+03	0	0	0	
-1.13097E+03	0			
-1.23402E-02	1.23402E-02			
-1.23402E-02	-1.23402E-02			
Constant				
5.25511E+17				

Station HUMP				
BHZ Channel				
Poles		Zeros		
Real	Imaginary	Real	Imaginary	
-5.02655E+02	0	0	0	
-1.00531E+03	0	0	0	
-1.13097E+03	0			
-1.23402E-02	1.23402E-02			
-1.23402E-02	-1.23402E-02			
Constant				
5.19041E+17				

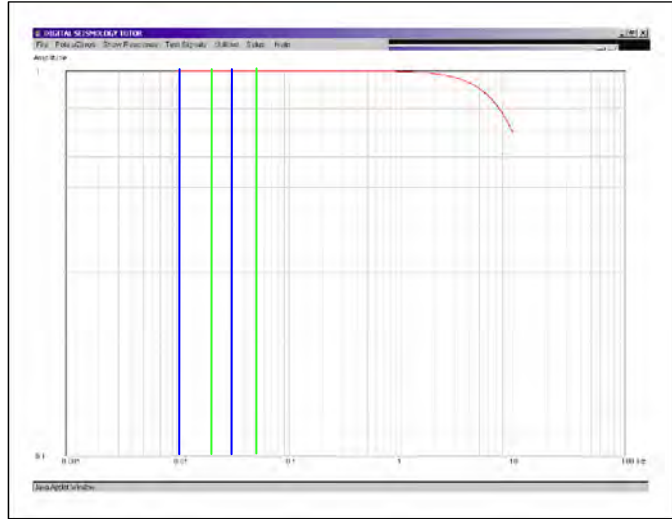


B.6 Instrument response for the PRSN broadband station MPR. The station was normalized to 1. Blue and Green lines represent the frequency bandpass utilized in the RMT inversion.

Station MPR BHE Channel			
Poles		Zeros	
Real	Imaginary	Real	Imaginary
-5.02655E+02	0	0	0
-1.00531E+03	0	0	0
-1.13097E+03	0		
-1.23402E-02	1.23402E-02		
-1.23402E-02	-1.23402E-02		
Constant			
7.14333E+17			

Station MPR BHN Channel			
Poles		Zeros	
Real	Imaginary	Real	Imaginary
-5.02655E+02	0	0	0
-1.00531E+03	0	0	0
-1.13097E+03	0		
-1.23402E-02	1.23402E-02		
-1.23402E-02	-1.23402E-02		
Constant			
5.30543E+17			

Station MPR BHZ Channel			
Poles		Zeros	
Real	Imaginary	Real	Imaginary
-5.02655E+02	0	0	0
-1.00531E+03	0	0	0
-1.13097E+03	0		
-1.23402E-02	1.23402E-02		
-1.23402E-02	-1.23402E-02		
Constant			
7.08579E+17			

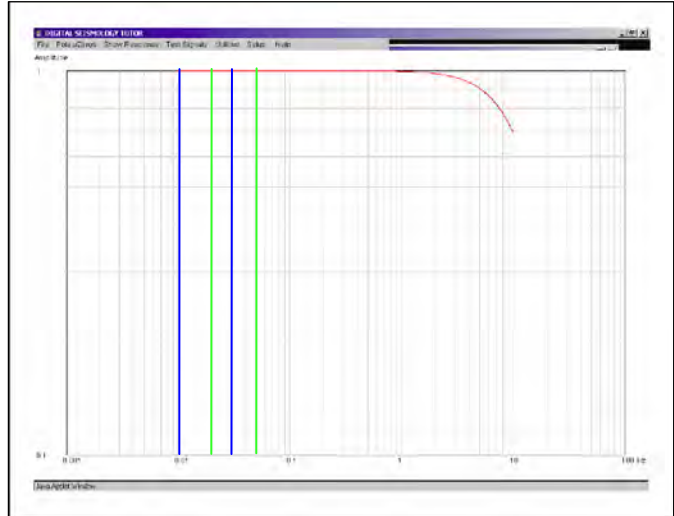


B.7 Instrument response for the GSN broadband station SJG. The station was normalized to 1. Blue and Green lines represent the frequency bandpass utilized in the RMT inversion.

Station SJG			
BHE Channel			
Poles		Zeros	
Real	Imaginary	Real	Imaginary
-1.23400E+02	1.23400E+02	0	0
-1.23400E+03	-1.23400E+02	0	0
-39.1800E+03	49.1200		
-39.1800E-02	-49.1200		
Constant			
3.78265E+12			

Station SJG			
BHN Channel			
Poles		Zeros	
Real	Imaginary	Real	Imaginary
-1.23400E+02	1.23400E+02	0	0
-1.23400E+03	-1.23400E+02	0	0
-39.1800E+03	49.1200		
-39.1800E-02	-49.1200		
Constant			
3.79921E+12			

Station SJG			
BHZ Channel			
Poles		Zeros	
Real	Imaginary	Real	Imaginary
-1.23400E+02	1.23400E+02	0	0
-1.23400E+03	-1.23400E+02	0	0
-39.1800E+03	49.1200		
-39.1800E-02	-49.1200		
Constant			
4.18344E+17			



APPENDIX C RMT INVERSION CODE

```
# ** RUNINV shell script **C.Mendoza: Jun2001
## Runs RMT inversion when data are in SAC format with "A" marker
## preset to first P arrival. Also, GMT plotting has been removed.
## Script uses version of data.csh that assumes SAC data from IRIS
## in velocity (m/s)

# To run: %runinv dirname datatype
#     where dirname refers to preexisting directory
#     that contains SAC data files and station list
#     and datatype refers to the type of data used
#     ("bb" for broadband and "lp" for long period)

date
cp prem.mod $1/in.mod
cp synth.csh $1/
cp dataSAC$2.csh $1/data.csh
cp wallnew $1/wall
cp plot.mac $1/
cd $1
echo 'RUNNING SHELL SCRIPT DATA.CSH'
csh data.csh
#
#Run the program 'wall' to generate the shell 'dosynth.csh'
#and the input file (infile) for the inversion routine (mtinv).
#The shell 'dosynth.csh' generates the synthetics and includes
#the parameters (distance, azimuth, name) of the stations
#to be considered in the inversion routine.
#NOTE: the version of wall used here reads station distance,azimuth
# directly from station.lst file and assumes a fixed depth of 10 km
#
./wall<<endwall
28.0
endwall
#
echo 'RUNNING SHELL SCRIPT DOSYNTH.CSH'
#Shell script SYNTH.CSH must exist in working directory
csh dosynth.csh
#
echo 'RUNNING INVERSION PROGRAM MTINV'
```

```

../mtinv<<endinv
infile
outfile
endinv
#
#Se grafican los resultados: sismogramas observado y sintetico para cada
#una de las estaciones/components.
#echo 'RUNNING SAC TO PLOT THE INVERSION RESULTS'
/data2/sac/bin/sac2000 <<endsac
macro plot.mac
endsac
/data2/sac/utls/sgftops f001.sgf f001.ps
/data2/sac/utls/sgftops f002.sgf f002.ps
/data2/sac/utls/sgftops f003.sgf f003.ps
/data2/sac/utls/sgftops f004.sgf f004.ps
/data2/sac/utls/sgftops f005.sgf f005.ps
/data2/sac/utls/sgftops f006.sgf f006.ps
#
mkdir out
mv *.dsp.* *.d.* *.clv *.vds *.vss mspec_* out/
mv *.csh inp_mod fort.* *file out/
mv plot.mac *.ps out/
rm wall in.mod *.sgf
echo 'DONE'
date
exit

```

APPENDIX D CRUSTAL STRUCTURES USED IN THE REGIONAL WAVEFORMS INVERSIONS

D.1 Caribbean Velocity Model (Ewing et. al., 1968)

Thickness (km)	V_P (km/sec)	V_S (km/sec)	Density (g/cm ³)
5	6.0	3.4	2.6
10	7.0	4.0	3.0
-	8.1	4.5	3.4

D.2 Preliminary Reference Earth Model (PREM) (Dziewonski & Anderson, 1981)

Thickness (km)	V_P (km/sec)	V_S (km/sec)	Density (g/cm ³)
3	5.79	3.19	2.60
15	6.79	3.89	2.90
25	8.10	4.48	3.38
40	8.09	4.47	3.37
60	8.08	4.46	3.37
80	8.07	4.45	3.37
-	8.01	4.38	3.37